3

HEAT TRANSPORT IN A RANDOMLY PACKED BED

3.1 INTRODUCTION

Heat transfer in a PBR can be divided into heat transfer in the axial direction and heat transfer in the radial direction. The coolant (helium) transfers the heat to the application (e.g. turbine) by forced convection (axial). In addition, heat losses from the core are unavoidable and should be optimized to fulfil certain operational and severe accident design conditions (radial). The heat transfer in the axial direction is usually dominated by forced convective heat transport due to fluid flow, although conduction and radiation may be present. The heat transfer in the radial direction occurs mainly due to a combination of a number of heat transfer mechanisms acting simultaneously, defined as the effective thermal conductivity.

Effective thermal conductivity in a high temperature PBR is derived by combining all of the parameters of relevant heat transfer mechanisms into a single representative value. This value is used to calculate the heat transfer in the radial direction under normal operation and severe upset conditions. According to Bauer (1990:2.8.1–1) the concept of total effective thermal conductivity of a packed bed k_{bed} can be split into three major components as discussed below.

The first component is that of the effective thermal conductivity k_{eff} in the bulk, near-wall and wall regions. This component is the combination of several distinct heat transfer mechanisms: (1) conduction through the solid; (2) conduction through the contact area between adjacent spheres accounting for surface roughness; (3) conduction through the stagnant fluid/gas phase; and (4) thermal radiation between touching and non-touching solid surfaces; (5) conduction between spheres and wall interface; (6) conduction through the gas phase in the wall region; and (7) thermal radiation between spheres touching and not touching the wall interface. This is illustrated graphically in Figure 3.1.

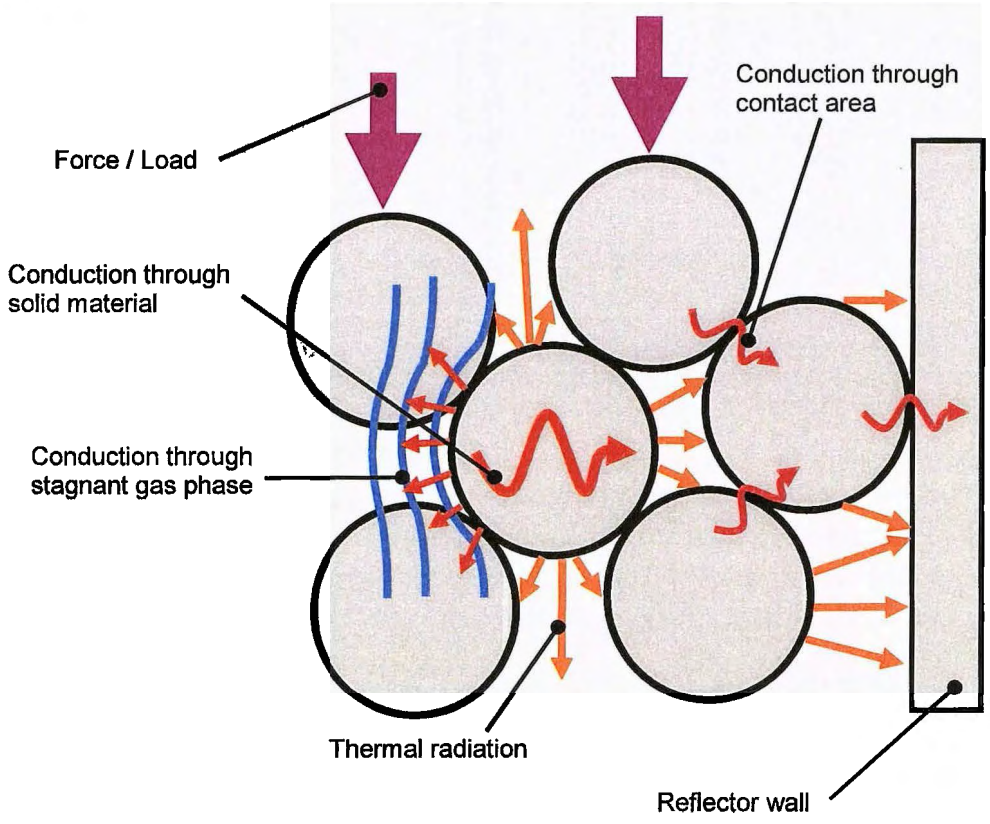

Figure 3.1: Heat transfer mechanisms through packed bed

It is to be emphasised that a distinction is made between conduction through point contact and conduction through a contact area in this study. Conduction through point contact refers to the situation in which no force is exerted on the pebble, which means that no deformation is present, only a very small contact point. However, conduction through a contact area refers to the situation in which an external force is exerted on a pebble, resulting in a larger contact area. Lu (2000:xix) investigated the increase in conduction due to an external force in much detail and found that the effective thermal conductivity of metal spheres in packed beds could increase by a factor of four times over a relatively small range of applied load (~1 MPa).

The second component is that of enhanced fluid effective thermal conductivity $k_{f,eff}$ due to the turbulent mixing of the fluid flowing through the voids of the packing in parallel with the wall while the solid phase is motionless. This is also referred to as the braiding effect. This turbulent mixing can be described as moving turbulent fluid pockets, flowing in a random manner. Each of these pockets transports energy and ultimately has the effect of increasing the effective thermal conductivity k_{bed} through the packed bed.

The third component is when the gas/fluid phase and the solid phase are in motion $k_{s,eff}$ caused by stirring or vibrations in the packing or by continuous fuelling and circulation in a

high temperature gas cooled nuclear reactor case. Therefore, there is additional heat transfer occurring via the solid phase due to the motion of the spheres. The relation is therefore given by Bauer (1990:2.8.1–1) as:

$$k_{bed} = k_{eff} + k_{f,eff} + k_{s,eff} \tag{3.1}$$

The focus of this study, however, is to review different methodologies in order to simulate the first component k_{eff} only, of the total effective thermal conductivity k_{bed}.

Traditionally, models simulating the effective thermal conductivity k_{eff} fall into two categories namely deterministic and statistical. The deterministic approach assumes the porous medium to consist of spheres arranged in a specific geometric configuration and based on this geometry, the effective thermal conductivity is calculated. The statistical approach, however, treats various microstructural formations statistically when applied to a randomly packed bed (Lu, 2000:12).

Before discussing the aforementioned two categories, we must define certain parameters influencing the effective thermal conductivity. Tsotsas & Martin (1987:23) define a primary and secondary parameter set. The primary parameters are the thermal conductivity of the solid (dispersed) phase k_s, the thermal conductivity of the fluid (continuous) phase k_f, and the variation in the porosity ε of a packed bed. Tsotsas & Martin (1987:23) stated that for a randomly packed bed consisting of equal-sized spheres the porosity ε is the only parameter needed to describe the structure of the packing. However, as shown in Chapter 2, systems with different arrangement (structure) usually have different effective thermal conductivities for the same porosity. The secondary parameters are related to the transport phenomena appearing mostly in packed beds with a gaseous fluid phase and are listed below:

1) Heat transfer through radiation k_e^r: this generally depends on temperature, optical properties of the surfaces and fluid, distance between surfaces and pebble diameter.

2) Pressure dependence of the thermal conductivity in dilute gases: the thermal conductivity of dilute gases is, according to the molecular theory of gases, independent of pressure. This is valid only on condition that the mean free path length λ of the gas molecules is small compared to the geometrical dimension d of the corresponding voids. Smoluchowski (1898:100) discovered this effect as early as 1898 and therefore this phenomenon is addressed as the Smoluchowski effect in this study. It has become common use to define the Smoluchowski effect with the Knudsen number. The Knudsen number is defined as the mean free path λ of the gas molecules divided by the geometrical dimension d of the corresponding voids

$Kn = \lambda/d$. The *mean free path* is defined as the average distance a gas molecule travels before it collides with another gas molecule, and is proportional to the gas temperature and inversely proportional to the gas pressure (Kennard, 1938:311).

According to Springer (1971:163) the heat transfer in a gas layer between two parallel plates is categorised into four regimes: continuum, temperature jump or slip, transition and free molecular. The Smoluchowski effect is illustrated by Bahrami *et al.* (2004:318) using a variance in heat flux with a change in the inverse of the Knudsen number, as illustrated in Figure 3.2.

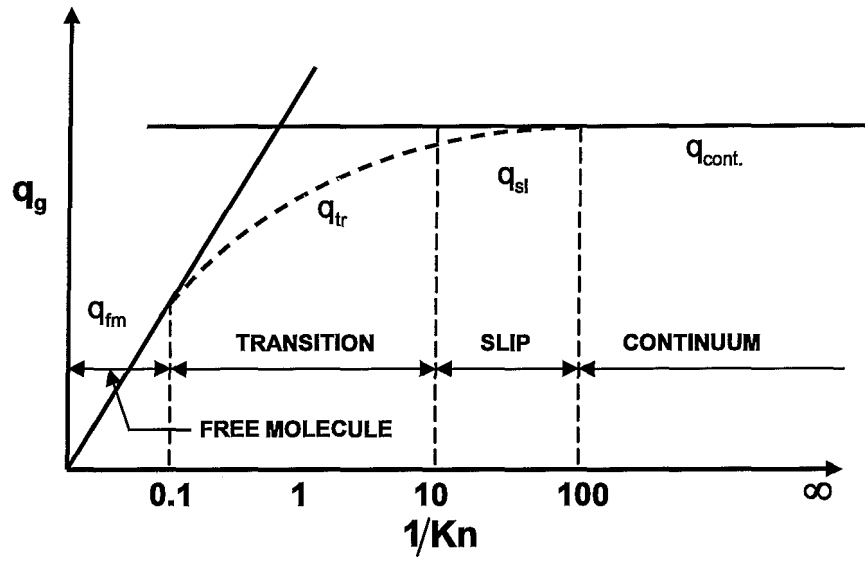

Figure 3.2: Heat transfer due to pressure dependence (Bahrami *et al.*, 2004:318)

3) Solid-to-solid heat transfer due to deformation of contact points: This can occur due to some external mechanical load or to the weight of the bed itself. Therefore, it can be argued that the extent of heat transfer in packed beds depends, *inter alia*, on the load, mechanical properties of the solid and surface roughness of the spheres.

Thus, the effective thermal conductivity in a randomly packed bed is a function of the following parameters:

$k_{eff} = f(k_s, k_f, \varepsilon, P_F, P_g, T, d_p,$ mechanical and optical properties of spheres (radiation), thermodynamic and optical properties of gas, pebble flattening) (3.2)

where k_s is the conductivity of the solid [W/mK], k_f the conductivity of the fluid [W/mK], ε the porosity, P_F is an external pressure [Pa] (force) on the spheres, P_g the fluid pressure [kPa], T the temperature [K] at the point of interest and d_p the pebble diameter.

3.2 DETERMINISTIC AND RESISTANCE MODELS

In this study, the effective thermal conductivity k_{eff} is divided into three components to independently illustrate its importance in the broader picture. The following summations give the total effective thermal conductivity k_{eff} :

$$k_{eff} = k_e^g + k_e^c + k_e^r \tag{3.3}$$

$$k_{eff} = k_e^{g,c} + k_e^r \tag{3.4}$$

where k_e^g is the effective thermal conductivity due to point contact conduction and conduction through the stagnant fluid, k_e^c is the effective thermal conductivity due to contact area, k_e^r is the effective thermal conductivity due to thermal radiation, and $k_e^{g,c}$ is the effective thermal conductivity due to point contact, stagnant fluid or gas and contact area.

3.2.1 SOLID AND FLUID EFFECTIVE THERMAL CONDUCTIVITY

In this section existing models accounting for the description/definition of the effective thermal conductivity due to point contact conduction at low temperatures are discussed. These models therefore exclude the effect of radiation between surfaces.

MODEL 1: Deissler & Boegli (1958:1417)

Deissler & Boegli (1958:1417) experimentally determined the effective thermal conductivity as early as 1958 in gas-saturated porous media. The solid phases used in their experiments included magnesium oxide, stainless-steel and uranium oxide powders, while the fluids included air, helium, argon, nitrogen and neon. Experiments were carried out with various mixtures of the different fluids. With these solid/fluid combinations, they obtained a range of results between $10 < \kappa < 1200$, where $\kappa = k_s/k_f$. These results were also obtained over two porosity ranges of $0.36 \leq \varepsilon \leq 0.405$ and $0.42 \leq \varepsilon \leq 0.50$ (Aichlmayr, 1999:31).

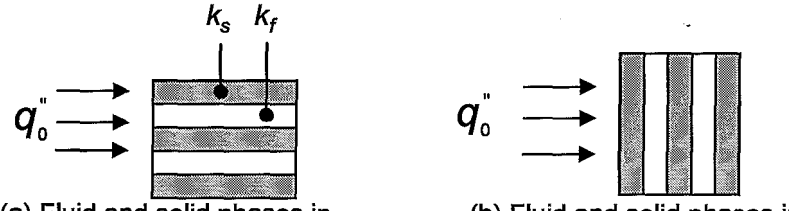

(a) Fluid and solid phases in parallel configuration

(b) Fluid and solid phases in series configuration

Figure 3.3: One-dimensional composite models (Aichlmayr, 1999:31)

Deissler & Boegli (1958:1417) note that the maximum effective thermal conductivity for a two-phase system is given by a unidirectional heat flow through parallel layers of solid/fluid phases (Figure 3.3(a)). The effective thermal conductivity for a parallel arrangement is given by:

$$k_e^{g,c} = \varepsilon k_f + (1-\varepsilon) k_s \tag{3.5}$$

which can be normalised by k_f and written in dimensionless form as:

$$\frac{k_e^{g,c}}{k_f} = \varepsilon + (1-\varepsilon)\kappa \tag{3.6}$$

Similarly, the minimum effective thermal conductivity occurs when the solid/fluid phases assume a series arrangement as shown in Figure 3.3 (b). The effective thermal conductivity for a series arrangement is then given by:

$$\frac{1}{k_e^{g,c}} = \frac{\varepsilon}{k_f} + \frac{(1-\varepsilon)}{k_s} \tag{3.7}$$

In dimensionless form, this arrangement yields:

$$\frac{k_e^{g,c}}{k_f} = \frac{1}{\varepsilon + \frac{(1-\varepsilon)}{\kappa}} \tag{3.8}$$

Thus, according to Deissler & Boegli (1958:1417) all effective thermal conductivity experimental data must fall inside the parallel and series layer bounds.

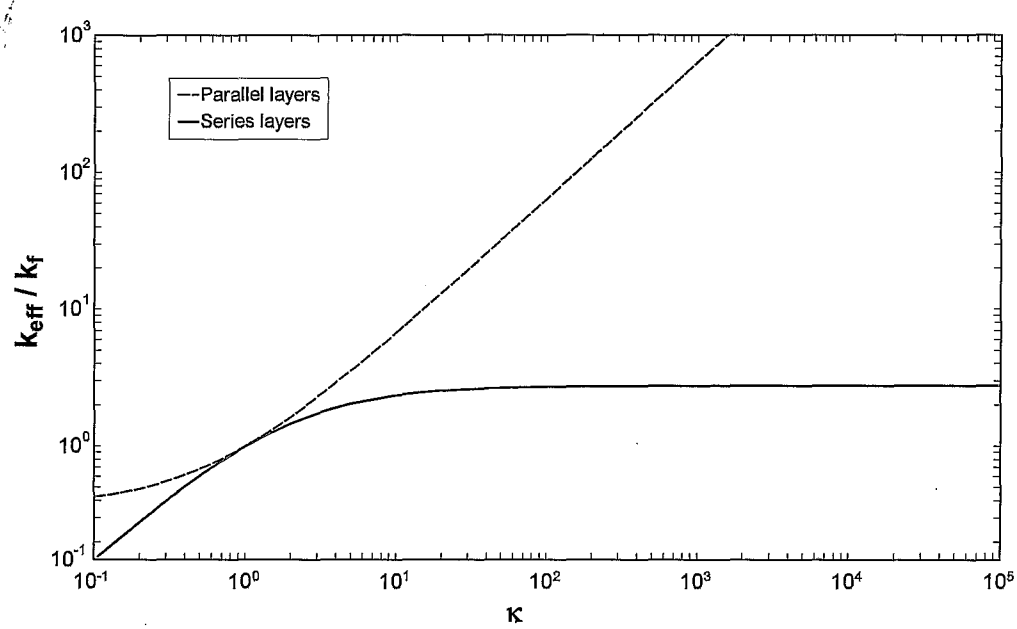

Figure 3.4: Parallel and Series layers (boundaries), $\varepsilon = 0.36$
Deissler & Boegli (1958:1417)

MODEL 2: Kunii & Smith (1960:71)

Kunii & Smith (1960:71) developed a model for heat transfer in packed beds considering unidirectional heat flow through two spheres in contact by lumping the solid/fluid heat transfer mechanisms. They analysed a packing arrangement by assuming that the heat transfer through the solid and fluid phases decomposes into separate modes acting in series and parallel. Their one-dimensional composite model, displayed in Figure 3.5, approximates the spherical pebble arrangement in a randomly packed bed. In order to calculate heat transfer through this spherical arrangement, Kunii & Smith (1960:72) defined effective lengths l_v, l_s and ΔL, which correspond to the lengths of the parallel and series regions. Consequently, ΔL is the total length between the two spheres.

Kunii & Smith (1960:72) noted that radiant heat transfer disappears when the void spaces contain liquid instead of gas and also when the spheres are relatively small and the temperature is below 482°C. Therefore, heat transfer through the void space is by conduction alone they argued, while heat transfer through the solid phase is comprised of a combination of parallel and series layers. The model displayed below accounts for the effective thermal conductivity due to conduction through the solid and gas/fluid phases alone. The correlations for the effective thermal conductivity due to radiation developed by Kunii & Smith (1960:71) are discussed in more detail later on.

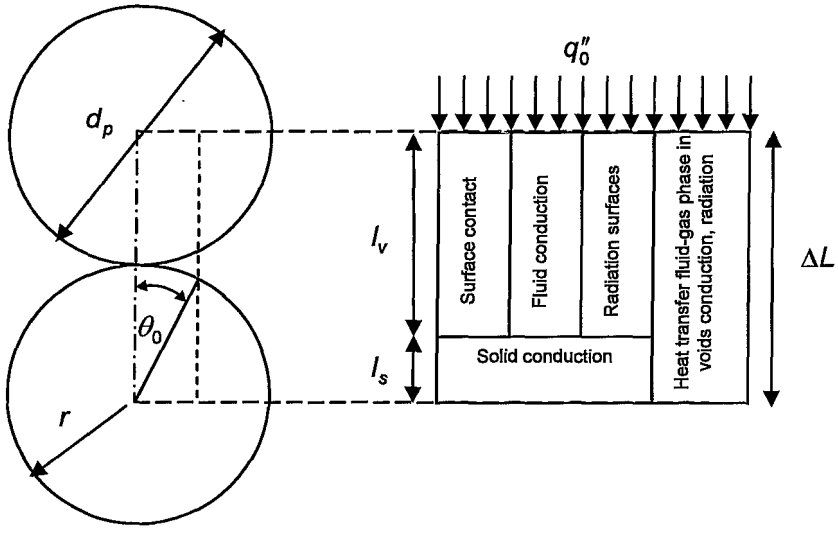

Figure 3.5: Kunii & Smith heat transfer model near the contact points1 (Kunii & Smith, 1960:71)

[1] Figure 2.8 in Aichlmayr (1999:36) and Figure16 in Aichlmayr & Kulacki (2006:407) are incorrect.

The effective thermal conductivity of the composite system is given finally by:

$$\frac{k_e^g}{k_f} = \varepsilon + \frac{\beta(1-\varepsilon)}{\psi_t + \frac{\gamma}{\kappa}} \tag{3.9}$$

It is necessary to know the empirical values of the three quantities β, γ and ψ_t when calculating the effective thermal conductivity. For a close packing of spheres, Kunii & Smith (1960:72) found an average value of $\beta = 0.895$. However, for most loose or open packings, β should be unity. Therefore, its value will range from 0.895 to 1 for almost all packed beds. The value of γ depends on l_s, and Kunii & Smith (1960:72) conclude that a value of $\gamma = 2/3$ is sufficient. In order to evaluate ψ_t, they assumed that a portion of the total heat transfer occurs through a single contact point. Thus, ψ_t is a function of the number of contact points between spheres and the thermal conductivities of the solid and fluid phases. Kunii & Smith (1960:74) corrected the coordination number, N_c to account only for those contact points responsible for heat transfer, defined in Chapter 2 as the coordination flux number n. For the basic loose packing, they argue that $n = 1.5$ and for a close packing $n = 4\sqrt{3}$, as previously mentioned in Chapter 2. ψ_t is then approximated by:

$$\psi_t = \psi_2 + (\psi_1 + \psi_2)\frac{\varepsilon - 0.260}{0.216} \qquad \text{for } 0.260 \le \varepsilon \le 0.476 \tag{3.10}$$

where ψ_1 and ψ_2 correspond to ψ_{1or2}, evaluated for the loose and close packing arrangements respectively, where ψ_{1or2} is given by[2]:

$$\psi_{1or2} = \frac{1}{2}\frac{\left(\frac{\kappa-1}{\kappa}\right)^2 \sin^2\theta_0}{\ln\left(\kappa-(\kappa-1)\cos\theta_0\right) - \left(\frac{\kappa-1}{\kappa}\right)(1-\cos\theta_0)} - \frac{2}{3}\frac{1}{\kappa} \tag{3.11}$$

where θ_0 [radians] is the fraction of the total heat transfer associated with one contact point between two spheres as displayed in Figure 3.5. This angle can be calculated by:

$$\sin^2\theta_0 = \frac{1}{n} \tag{3.12}$$

MODEL 3: Zehner & Schlünder (1970:933)

Zehner & Schlünder (1970:933) considered the effective thermal conductivity between two

[2] Noted by Aichlmayr (1999:36) that in Kunii and Smith (1960:73) l_n instead of ln appears in Eq. (3.11). This is apparently a misprint because l_n does not appear anywhere else in Kunii and Smith's (1960:73) paper.

spheres by considering a cylindrical unit cell containing both solid and fluid/gas phases. One-eighth of a sphere (unit cell) is presented in Figure 3.6.

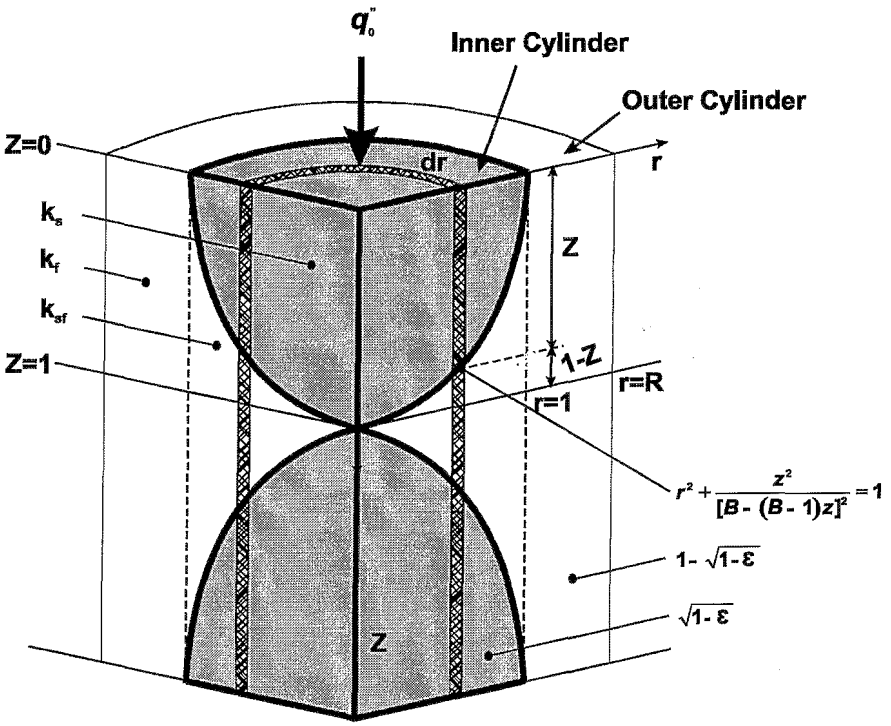

Figure 3.6: Zehner & Schlünder unit cell model
(Zehner & Schlünder, 1970:933)

The unit cell contains an inner cylinder of $0 \le r \le 1$, whiles the remaining volume of $1 < r \le R$, is occupied by a fluid or gas phase only. Zehner & Schlünder (1970:933) further assumed that heat transfer occurs in parallel paths through the inner cylinder and outer annulus; thus, the effective thermal conductivity of the unit cell is given by:

$$k_e^g = \left(1-\frac{1}{R^2}\right)k_f + \frac{1}{R^2}k_{sf} \tag{3.13}$$

where k_{sf} is the effective thermal conductivity of the inner cell consisting of both the solid and fluid phases in series and an unknown parameter R. From mass transfer experiments investigated by Zehner & Schlünder (1970:933), the diffusivity ratio of a bed saturated with fluid to that of a pure fluid (gas) is related to the porosity by:

$$\frac{D_e}{D_f} = 1-\sqrt{1-\varepsilon} \tag{3.14}$$

where D_e is the diffusivity of a fluid/gas-saturated packed bed and D_f is the diffusivity of the fluid or gas phase only. Drawing an analogy between mass diffusion and thermal conduction, it is argued that when $k_s \to 0$:

$$\lim \frac{k_s}{k_f} \to 0 : \frac{k_e^g}{k_f} = \frac{D_e}{D_f} = 1 - \sqrt{1-\varepsilon} \tag{3.15}$$

The function given in Eq. (3.15) was obtained by curve-fitting through experimental data displayed in Figure 3.7 (a). It is important to note that structured packings were used to achieve a certain magnitude of porosity. Therefore, this model would be more accurate in the bulk region where structured packings is a more accurate representation of a randomly packed bed, than in the near-wall region where structured packings fail to represent a random packing as previously mentioned in Section 2.4.

Figure 3.7 (b) displays experimental results where electrical conduction through the test sections was used, as opposed to the diffusivity of fluids. One can argue that the $1-\sqrt{1-\varepsilon}$ curve-fit function in Figure 3.7 (b) under-predicts the conductivity through the fluid phase compared to the experimental results.

Tsotsas & Martin (1987:22) note that the advantages of the electrical conductivity method are the great accuracy with which electric quantities can be measured and the freedom from any natural convection. However, its main shortcoming is that certain features of heat transfer in packed beds with a gaseous fluid phase cannot be simulated with electrical systems; this holds for the thermal radiation, as well as for the pressure dependence of the thermal conductivity of the gas in confined spaces.

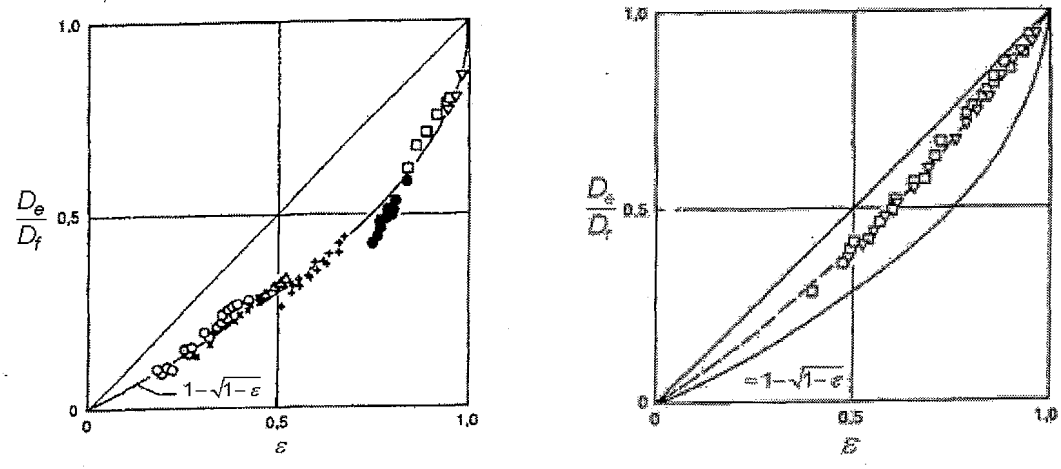

(a) with diffusivity of fluids (b) with electrical conduction through fluid

Figure 3.7: Zehner & Schlünder curve fit through diffusivity experiments (Zehner & Schlünder, 1970:933)

Assuming a series configuration in the thermal resistances of the solid and gas phases in the inner cylinder, it can be deduced that $k_{sf} \to k_s$ as $k_s / k_f \to 0$ (Zehner & Schlünder, 1970:933). Under such conditions, a comparison of Eq. (3.13) and Eq. (3.15) yields:

$$\frac{1}{R^2} = \sqrt{1-\varepsilon} \tag{3.16}$$

From Eq. (3.13) and Eq. (3.16), it is found that:

$$k_e^g = \left(1-\sqrt{1-\varepsilon}\right)k_f + \sqrt{1-\varepsilon}\,k_{sf} \tag{3.17}$$

In order to determine k_{sf}, the inner cylinder is assumed to have an arbitrary shape given by:

$$r^2 + \frac{z^2}{\left[B-(B-1)z\right]^2} = 1 \tag{3.18}$$

where B is an empirical deformation parameter and z is a distance in the axial direction.

As previously mentioned, the thermal conductivity k_{sf} of the inner cylinder is related to the solid and fluid thermal conductivities through the assumption that both phases interact in series with each other. k_{sf} is then obtained by integrating the layer thermal conductivity over the inner cylinder volume to yield the following:

$$\frac{k_{sf}}{k_f} = \frac{2}{1-\kappa^{-1}B}\left[\frac{\left(1-\kappa^{-1}\right)B}{\left(1-\kappa^{-1}B\right)^2}\ln\left(\frac{1}{\kappa^{-1}B}\right) - \frac{B+1}{2} - \frac{B-1}{1-\kappa^{-1}B}\right] \tag{3.19}$$

Eq. (3.19) is then substituted into Eq. (3.17) to yield the effective thermal conductivity of the unit cell, which is given by:

$$\frac{k_e^g}{k_f} = \left[1-\sqrt{1-\varepsilon}\right] + \frac{2\sqrt{1-\varepsilon}}{1-\kappa^{-1}B}\left[\frac{\left(1-\kappa^{-1}\right)B}{\left(1-\kappa^{-1}B\right)^2}\ln\left(\frac{1}{\kappa^{-1}B}\right) - \frac{B+1}{2} - \frac{B-1}{1-\kappa^{-1}B}\right] \tag{3.20}$$

The deformation parameter appearing in Eq. (3.18) has limiting values. For $B=1$, Eq. (3.18) describes the surface of a sphere, $B<1$ more or less represents prolongated needles and for $B>1$ barrel-like bodies are obtained. The deformation of the spheres B is related to porosity by:

$$\varepsilon = 1-\left(\frac{B\left(3-4B+B^2+2\ln B\right)}{(B-1)^3}\right)^2 \tag{3.21}$$

A good explicit approximation of Eq. (3.21) is:

$$B = C\left(\frac{1-\varepsilon}{\varepsilon}\right)^m \tag{3.22}$$

Zehner & Schlünder (1970:933) recommended $C = 1.25$ and $m = 10/9$ for Eq. (3.22). Later, Hsu *et al.* (1994:2751) found that $C = 1.364$ and $m = 1.055$ resulted in a more accurate approximation (Aichlmayr, 1999:40).

MODEL 4: Okazaki et al. (1977:164)

Okazaki *et al.* (1977:164; as quoted by Okazaki *et al.*, 1981:183) derived a model using the same process as Kunii & Smith (1960:71). However, one distinct difference is the use of the coordination flux number n to represent the heat path. Okazaki *et al.* (1977:164) related the average coordination number to porosity by using Ridgeway & Tarbuck's (1967:384) model presented in Eq. (2.13). The coordination flux number was calculated as:

$$n = \frac{\overline{N_c}}{6} \tag{3.23}$$

Okazaki *et al.* (1977:164) assumed a unit cell consisting of a solid part and a macro-void part, as displayed in Figure 3.8. The fractional areas of the solid part and the macro-void part across which the heat transfer occurs are given in Table 3.1.

Table 3.1: Areas of solid and macro-void part at various porosities

$\varepsilon \geq 1/3$		$\varepsilon < 1/3$	
A_s	A_v	A_s	A_v
$3(1-\varepsilon)/2$	$(3\varepsilon-1)/2$	1	0

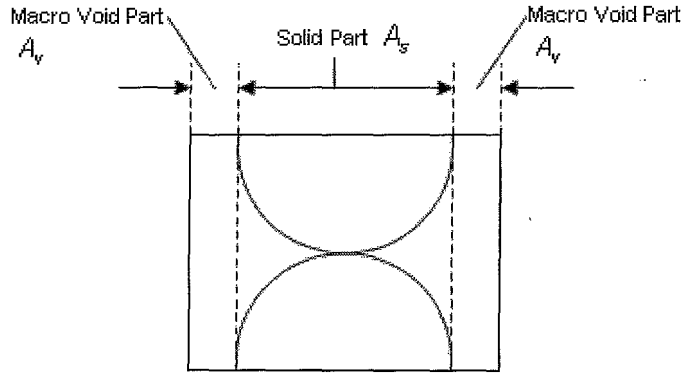

Figure 3.8: Okazaki et al. unit cell model of packed bed (Okazaki et al., 1977:164)

The apparent thermal conductivity of the solid part k_{es} is given as follows with θ_0 in radians:

$$\frac{k_{es}}{k_f} = 2n\left(\frac{\kappa}{\kappa-1}\right)^2\left[\ln\left(\kappa-(\kappa-1)\cos\theta_0\right)\right]-\left(\frac{\kappa-1}{\kappa}\right)(1-\cos\theta_0) \tag{3.24}$$

where

$$\sin^2\theta_0 = \frac{1}{n} \tag{3.25}$$

Then the effective thermal conductivity k_e^g of the granular bed is given by:[3]

$$\frac{k_e^g}{k_f} = A_v k_s + A_s k_s \left(\frac{k_{es}}{k_f}\right) \tag{3.26}$$

MODEL 5: Batchelor & O'Brien (1977:313)

Batchelor & O'Brien (1977:313) derived an equation with the focus on pebble-to-pebble contact that approximates the effective thermal conductivity when $\kappa \geq 1$. They assumed an analogy between electrical conductivity and thermal conductivity. Three limiting cases were under consideration for contact between spheres: point contact, no contact and contact area due to pebble deformation.

They also found that the dominant factor for heat transfer at relatively low temperatures is the coordination number. They noted that much controversy exists in the comparison between coordination number and porosity. However, after much consideration they adopted an average coordination number of $\overline{N}_C = 6.5$, as suggested by Adams & Matheson (1972:1989). Batchelor & O'Brien (1977:313) further found that for spheres with a large thermal conductivity, almost all of the heat flux through the spheres occurs through the flattened regions resulting from local pebble deformations. Hence, the pebble-to-pebble contact area significantly affects the effective thermal conductivity through a packed bed.

With all these observations, they were able to derive a model for k_e^g based upon combining the solid and fluid effective thermal conductivity with the effect of pebble-to-pebble area conduction given as:

$$\frac{k_e^g}{k_f} = 4.0 \ln\left(\frac{k_s}{k_f}\right) \tag{3.27}$$

They emphasised that Eq. (3.27) is the leading term in an asymptotic expansion of k_e^g / k_f as $\kappa \to \infty$, and that the next term is a constant of order unity that depends on the (statistical) geometry of the arrangement of the spheres. Batchelor & O'Brien (1977:313) used Eq. (3.27) and empirically fitted a curve through experimental data obtaining:

[3] Okazaki *et al.* (1981:183) did not divide k_{eff} with k_f in Eq. (3.24); it was presented by Abou-Sena *et al.* (2007:206).

$$\frac{k_e^g}{k_f} = 4.0 \ln\left(\frac{k_s}{k_f}\right) - 11 \tag{3.28}$$

While Eq. (3.28) is not an explicit function of porosity due to the assumed packing arrangement, Batchelor & O'Brien (1977:313) argued that even though k_e^g depends rather strongly on the coordination number, small porosity variations may be neglected with little error. Thus, the validity of the Batchelor & O'Brien (1977:313) correlation is limited to the bulk porosity region of a packed bed.

MODEL 6: Hsu et al. (1995:264) Two-dimensional (Square Cylinder Model)

Based on the one-dimensional lumped parameter model of Kunii & Smith (1960:71), Hsu *et al.* (1995:264) developed three lumped parameter models to calculate the effective thermal conductivity in porous media. Hsu *et al.* (1995:265) first considered a two-dimensional unit cell model comprised of contacting square cylinders. This model is based on the simplified discontinuous fluid phase model of Nozad *et al.* (1985a:843) with symmetry arguments, which is displayed graphically in Figure 3.9.

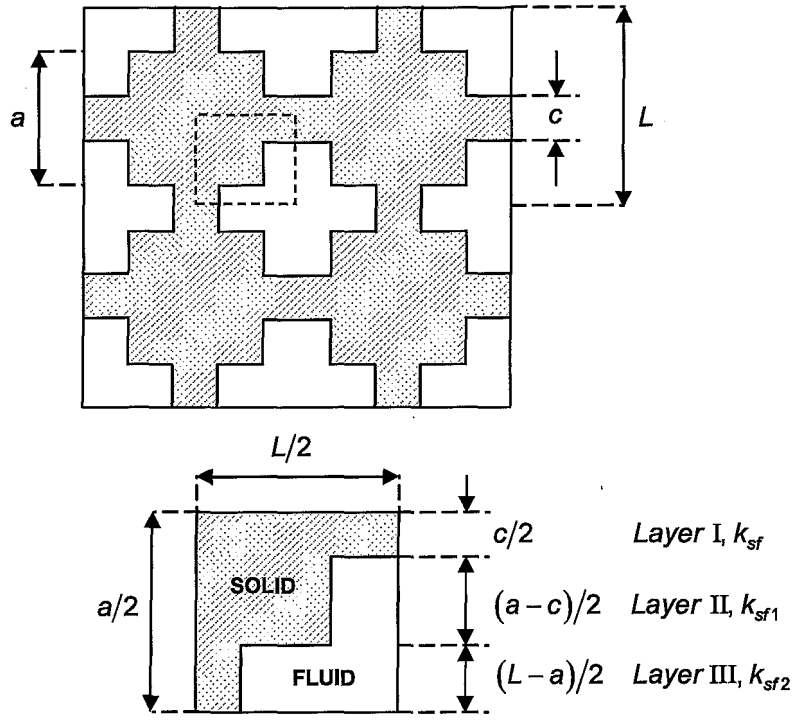

Figure 3.9: (a) An array of touching square cylinders (above) and (b) its unit cell (below) (Hsu *et al.*, 1995:265)

Hsu *et al.* (1995:265) argued that the unit cell consists of three parallel layers, as displayed in Figure 3.9 (b). Considering this arrangement, the effective thermal conductivity of the three layers is given by:

$$k_e^{g,c} = \gamma_a \gamma_c k_s + \gamma_a (1-\gamma_c) k_{sf1} + (1-\gamma_a) k_{sf2} \tag{3.29}$$

where k_{sf1} and k_{sf2} are the thermal conductivities of the composite layers, $\gamma_a = a/L$ and $\gamma_c = c/a$. The values of k_{sf1} and k_{sf2} are then obtained by the layer in series method, which is given below:

$$\frac{1}{k_{sf1}} = \frac{a/L}{k_s} + \frac{(1-a)/L}{k_f} \tag{3.30}$$

where a is the length of one side of the solid square cube, c is the width of the connecting plate and L is the length of the unit cell. This can be rewritten in non-dimensional form as:

$$\frac{k_{sf1}}{k_f} = \frac{1}{1+\left(\kappa^{-1}-1\right)\gamma_a} \tag{3.31}$$

Similarly, the value of k_{sf2} is given by:

$$\frac{k_{sf2}}{k_f} = \frac{1}{1+\left(\kappa^{-1}-1\right)\gamma_a\gamma_c} \tag{3.32}$$

Substituting Eq. (3.31) and Eq. (3.32) into Eq. (3.29) yields:

$$\frac{k_e^{g,c}}{k_f} = \gamma_a\gamma_c\kappa + \frac{\gamma_a(1-\gamma_c)}{1+\left(\kappa^{-1}-1\right)\gamma_a} + \frac{(1-\gamma_a)}{1+\left(\kappa^{-1}-1\right)\gamma_a\gamma_c} \tag{3.33}$$

The geometric parameter γ_a is related to the porosity and the adjustable parameter γ_c through:

$$1-\varepsilon = \gamma_a^2 + 2\gamma_c\gamma_a(1-\gamma_a) \tag{3.34}$$

where γ_c is the same parameter used by Nozad *et al.* (1985a:843) in their numerical calculations. Nozad *et al.* (1985a:843) found that the numerical results compared closely with their experimental results when $\gamma_c = 0.02$. However, Shonnard & Whitaker (1989:503) point out that there is an error in the computations of Nozad *et al.* (1985a:843) and that their numerical solution with $\gamma_c = 0.01$ would be more appropriate for representing the experimental data in Nozad *et al.* (1985b:857). Hsu *et al.* (1995:265) adjusted γ_c until agreement between Eq. (3.33) and experimental data from the literature was achieved. Hsu *et al.* (1995:265) found that $\gamma_c = 0.01$ and $\varepsilon = 0.36$ yield the best agreement with the experimental data obtained by Nozad *et al.* (1985b:857).

MODEL 7: Hsu et al. (1995:266) Two-dimensional (Circular Cylinder Model)

In this model, Hsu *et al.* (1995:266) considered a unit cell by replacing the connecting square cylinders presented in Figure 3.9 with an array of touching circular cylinders. The cylinders have diameter a and are connected by plates of thickness c and height h^*, as displayed in Figure 3.10. The plate height is given by:

$$\frac{h^*}{L} = 1 - \gamma_a \sqrt{1 - \gamma_c^2} \tag{3.35}$$

with $\gamma_a = a/L$ and $\gamma_c = c/a$. The contact angle is defined by:

$$\theta_c = \sin^{-1}(\gamma_c) \tag{3.36}$$

It should be noted that the geometric parameters are related to the porosity by:

$$\varepsilon = 1 - \gamma_c \gamma_a - \frac{\gamma_a^2}{2}\left(\frac{\pi}{2} - 2\theta_c\right) \tag{3.37}$$

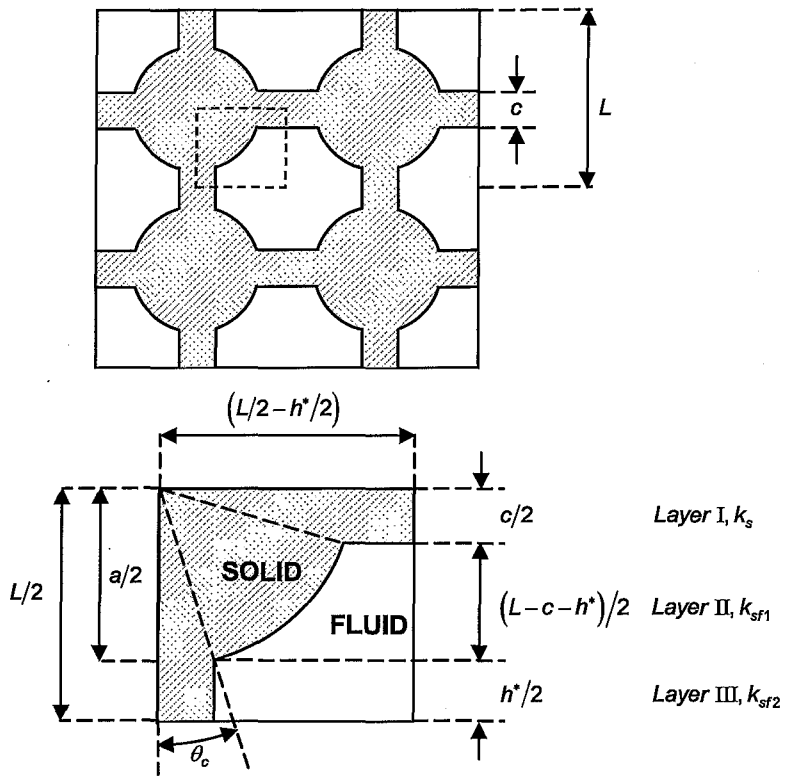

Figure 3.10: (a) An array of touching circular cylinders (above) and (b) the unit cell (below) (Hsu *et al.*, 1995:267)

Aichlmayr & Kulacki (2006:437) note that the aforementioned equation, Eq. (3.35), was not presented in Hsu *et al.* (1995:266). The effective thermal conductivity of the unit cell is found by assuming that Layers I, II, III in Figure 3.10 are parallel thermal resistances. Hence:

$$k_e^{g,c} = \frac{c}{L}k_s + \left(1 - \frac{c}{L} - \frac{h^*}{L}\right)k_{sf1} + \frac{h^*}{L}k_{sf2} \tag{3.38}$$

where k_{sf1} and k_{sf2} are the effective thermal conductivities of Layers II and III. The layer conductivities are given by:

$$\frac{k_{sf1}}{k_f} = \frac{1}{\gamma_a\left(\sqrt{1-\gamma_c^2} - \gamma_c\right)}\left[\left(\frac{\kappa}{1-\kappa}\right)\left(\frac{\pi}{2} - 2\theta_c\right) - \left(\frac{\kappa}{1-\kappa}\right)\int_{\theta_c}^{\pi/2-\theta_c} \frac{d\theta}{1+\left(\frac{1}{\kappa}-1\right)\gamma_a \sin\theta}\right] \tag{3.39}$$

and

$$\frac{k_{sf2}}{k_f} = \frac{1}{1+\left(\frac{1}{\kappa}-1\right)\gamma_a\gamma_c} \tag{3.40}$$

respectively. The last integral in Eq. (3.39) can be integrated depending on whether $(1/\kappa - 1)\gamma_a$ is less than, equal to, or larger than one. Consequently, computing Eq. (3.39) and substituting the result and Eq. (3.40) into Eq. (3.38) yields three expressions:

(i) For $(1/\kappa - 1)\gamma_a < 1$

$$\frac{k_e^{g,c}}{k_f} = \gamma_c\gamma_a\kappa + \frac{1-\gamma_a\sqrt{1-\gamma_c^2}}{\gamma_a\gamma_c\left(\frac{1}{\kappa}-1\right)+1} + \frac{\kappa\left(\frac{\pi}{2}-2\theta_c\right)}{1-\kappa}$$
$$- \frac{2\kappa}{(1-\kappa)\sqrt{1-\left(\frac{1}{\kappa}-1\right)^2\gamma_a^2}}\left\{\tan^{-1}\left[\frac{\tan\left(\frac{\pi}{4}-\frac{\theta_c}{2}\right)+\left(\frac{1}{\kappa}-1\right)\gamma_a}{\sqrt{1-\left(\frac{1}{\kappa}-1\right)^2\gamma_a^2}}\right] - \tan^{-1}\left[\frac{\tan\left(\frac{\theta_c}{2}\right)+\left(\frac{1}{\kappa}-1\right)\gamma_a}{\sqrt{1-\left(\frac{1}{\kappa}-1\right)^2\gamma_a^2}}\right]\right\} \tag{3.41}$$

(ii) For $(1/\kappa - 1)\gamma_a > 1$

$$\frac{k_e^{g,c}}{k_f} = \gamma_c\gamma_a\kappa + \frac{1-\gamma_a\sqrt{1-\gamma_c^2}}{\gamma_a\gamma_c\left(\frac{1}{\kappa}-1\right)+1} + \frac{\kappa\left(\frac{\pi}{2}-2\theta_c\right)}{1-\kappa}$$
$$- \frac{\kappa}{(1-\kappa)\sqrt{\left(\frac{1}{\kappa}-1\right)^2\gamma_a^2-1}}\left\{\ln\left[\frac{\tan\left(\frac{\pi}{4}-\frac{\theta_c}{2}\right)+\left(\frac{1}{\kappa}-1\right)\gamma_a-\sqrt{\left(\frac{1}{\kappa}-1\right)^2\gamma_a^2-1}}{\tan\left(\frac{\pi}{4}-\frac{\theta_c}{2}\right)+\left(\frac{1}{\kappa}-1\right)\gamma_a+\sqrt{\left(\frac{1}{\kappa}-1\right)^2\gamma_a^2-1}}\right]\right.$$
$$\left.-\ln\left[\frac{\tan\left(\frac{\theta_c}{2}\right)+\left(\frac{1}{\kappa}-1\right)\gamma_a-\sqrt{\left(\frac{1}{\kappa}-1\right)^2\gamma_a^2-1}}{\tan\left(\frac{\theta_c}{2}\right)+\left(\frac{1}{\kappa}-1\right)\gamma_a+\sqrt{\left(\frac{1}{\kappa}-1\right)^2\gamma_a^2-1}}\right]\right\} \qquad (3.42)$$

(iii) For $(1/\kappa - 1)\gamma_a = 1$

$$\frac{k_e^{g,c}}{k_f} = \frac{\gamma_c\gamma_a^2}{\gamma_a+1} + \frac{1-\gamma_a\sqrt{1-\gamma_c^2}}{\gamma_c+1} + \gamma_a\left(\frac{\pi}{2}-2\theta_c\right) - \left[\tan\left(\frac{\pi}{4}-\frac{\theta_c}{2}\right)-\tan\left(\frac{\theta_c}{2}\right)\right] \qquad (3.43)$$

Hsu *et al.* (1995:267) found that $\gamma_c = 0.01$ yields the best agreement with the experimental data.

MODEL 8: Hsu et al. (1995:264) Three-dimensional (Cube Model)

Hsu *et al.* (1995:267) extended the touching Square Cylinder Model by considering a three-dimensional unit cell consisting of cubes, as displayed in Figure 3.11. Hsu *et al.* (1995:267) partitioned the unit cell into regions through which conduction is one-dimensional. The following relation for the Three-dimensional Cube Model is obtained:

$$\frac{k_e^{g,c}}{k_f} = 1-\gamma_a^2-2\gamma_c\gamma_a+2\gamma_c\gamma_a^2+\gamma_c^2\gamma_a^2\kappa+\frac{\gamma_a^2-\gamma_c^2\gamma_a^2}{\left[1-\gamma_a+\gamma_a\left(\frac{1}{\kappa}\right)\right]}+\frac{2\left(\gamma_c\gamma_a-\gamma_c\gamma_a^2\right)}{\left[1-\gamma_c\gamma_a+\gamma_c\gamma_a\left(\frac{1}{\kappa}\right)\right]} \qquad (3.44)$$

The geometric parameters γ_a and γ_c are related to porosity by:

$$1-\varepsilon = \left(1-3\gamma_c^2\right)\gamma_a^3+3\gamma_c^2\gamma_a^2 \qquad (3.45)$$

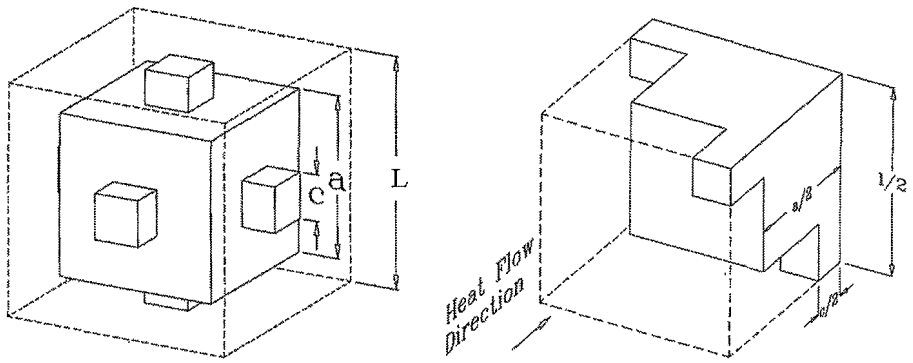

Figure 3.11: (a) In-line touching cubes (left) and (b) Hsu *et al.*'s unit cell (right) (Hsu *et al.*, 1995:268)

Hsu *et al.* (1995:267) recommended $\gamma_c = 0.01$ for the square and cylinder models and $\gamma_c = 0.13$ for the cube model with a porosity of $\varepsilon = 0.36$, in order to best approximate the experimental data and numerical results from Nozad *et al.* (1985a:843) and Nozad *et al.* (1985b:857).

MODEL 9: Cheng et al. (1999:4199)

Cheng *et al.* (1999:4199) presented an alternative approach to determining the effective thermal conductivity of a packed bed consisting of mono-sized spheres, in the presence of a stagnant fluid. They considered a packing structure in a microscopic manner with the Voronoi polyhedra (as was discussed in Section 2.2.6). However, in order to use this model, numerically generated coordinates of the packing structure must be obtained to calculate several of the Voronoi polyhedron parameters. Their focus was to derive a model with $T < 200°C$ by considering the following heat transfer mechanisms; conduction through the solid and conduction through the contact area between spheres. This was done by using numerical data of spherical or near spherical pebbles with porosities ranging from 0.35 to 0.41.

According to Cheng *et al.* (1999:4199), a number of neighbouring spheres of various shapes of Voronoi polyhedra influence the heat transfer between spheres. Therefore, they simplified the Voronoi polyhedra by assuming that the heat transfer between two neighbouring spheres occurs only in a double pyramid whose base is the Voronoi boundary plane and vertexes are the centres of the spheres (Figure 3.12 (a)). This heat transfer is not affected by the presence of other spheres and fluid. Further simplification was achieved by replacing the double pyramid with a double taper cone of the same volume and distance between the vertexes as the original Voronoi polyhedron (Figure 3.12 (b)).

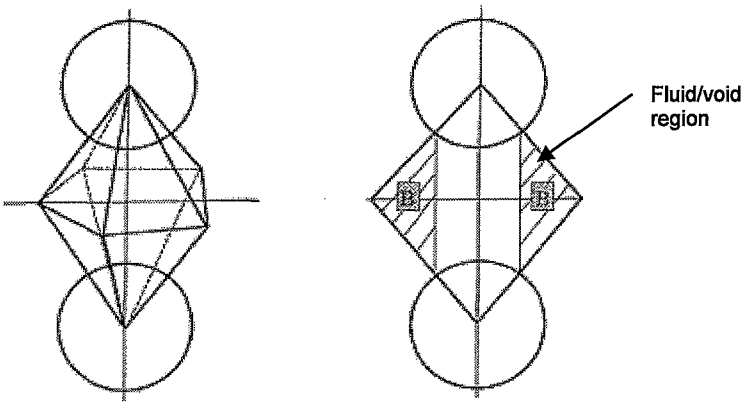

(a) A double pyramid model (b) A double taper cone model with shaded area as region B

Figure 3.12: Connection models between two neighbouring Voronoi polyherdra (Cheng *et al.*, 1999:4201)

This treatment led to a heat transfer problem that can be solved analytically. Two cases were identified for the derivation of their models between two neighbouring spheres *i* and *j*, with respective temperatures expressed as T_i and T_j, namely:

- Case 1: Two spheres are not or just in contact (Figure 3.13 (a) and (b)). The heat transfer path is the heat conduction through the solid spheres and stagnant fluid in between.
- Case 2: There is a contact area between two spheres, due to deformation (Figure 3.13 (c)). The heat transfer is through two parallel paths: the conduction through the solid spheres, with stagnant fluid in between, and the conduction through the contact area.

Cheng *et al.* (1999:4199) developed two different models based on both cases described above.

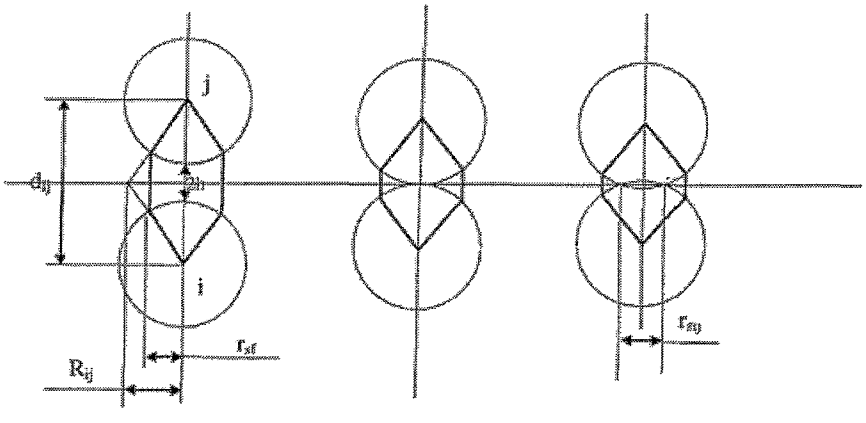

(a) Non-contact (b) Point-contact (c) Area-contact

Figure 3.13: Various contact conditions between two spheres (Cheng *et al.*, 1999:4201)

Model A:

This model assumes that the surface of the taper cone is isothermal, equal to its corresponding representative temperature and ignores conduction through the stagnant fluid in the void region B (Figure 3.12). In this case, the following equations were derived.

Case 1: If the direction of heat flow is parallel to the line connecting the centres of two spheres (Figure 3.13 (a)), then it can be shown that:

$$dQ_{ij} = \frac{2\pi r\, dr}{\frac{H_{1r}}{k_{si}} + \frac{H_{2r}}{k_f} + \frac{H_{3r}}{k_{sj}}}\left(T_i - T_j\right) \tag{3.46}$$

where the geometrical parameters (Figure 3.13 and Figure 3.14) are given by:

$$H_{1r} = H_{3r} = \sqrt{R_p^2 - r^2} - \frac{r\left(R_p + h\right)}{R_{ij}} \tag{3.47}$$

$$H_{2r} = 2\left[\left(R_p + h\right) - \sqrt{R_p^2 - r^2}\right] \tag{3.48}$$

$$R_{ij} = \sqrt{\frac{3V_{ij}}{\pi d_{ij}}} \tag{3.49}$$

$$h = \frac{\left(d_{ij} - 2R_p\right)}{2} \tag{3.50}$$

where V_{ij} and d_{ij} are parameters that can be determined from a known packing structure. Q_{ij} is then given by:

$$Q_{ij} = \left(T_i - T_j\right) \times \int_0^{r_{sf}} \frac{2\pi r}{\left(\sqrt{R_p^2 - r^2} - \frac{r\left(R_p + h\right)}{R_{ij}}\right)\left(\frac{1}{k_{si}} + \frac{1}{k_{sj}}\right) + \frac{2\left(\left(R_p + h\right) - \sqrt{R_p^2 - r^2}\right)}{k_f}} dr \tag{3.51}$$

where

$$r_{sf} = R_p \frac{R_{ij}}{\sqrt{R_{ij}^2 + \left(R_p + h\right)^2}} \tag{3.52}$$

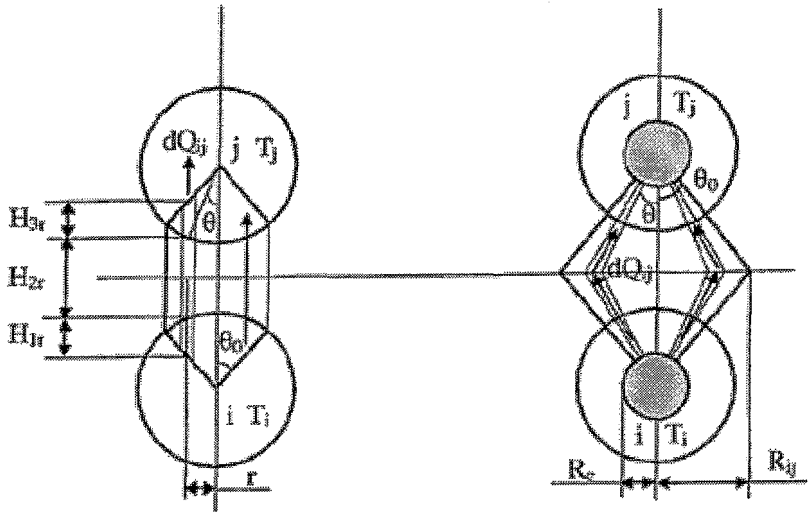

(a) Model A (b) Model B

Figure 3.14: Heat conduction model between two neighbouring Voronoi polyhedra (Cheng *et al.*, 1999:4204)

Case 2: In this case there are two parallel paths for the heat transfer between two spheres: the conduction through the solid spheres and the stagnant fluid in between denoted Q_{ij1} and the conduction through the contact area between spheres Q_{ij2}, so that:

$$Q_{ij} = Q_{ij1} + Q_{ij2} \tag{3.53}$$

Similar to *Case 1* but with different integration boundaries, the heat flux through the stagnant fluid is given by:

$$Q_{ij} = \left(T_i - T_j\right) \times \int_{r_{sij}}^{r_{sf}} \frac{2\pi r}{\left(\sqrt{R_p^2 - r^2} - \frac{r\left(R_p + h\right)}{R_{ij}}\right)\left(\frac{1}{k_{si}} + \frac{1}{k_{sj}}\right) + \frac{2\left(\left(R_p + h\right) - \sqrt{R_p^2 - r^2}\right)}{k_f}} dr \tag{3.54}$$

The heat flux through the contact area of the two spheres is calculated by a slightly modified version of the model developed by Batchelor & O'Brien (1977:313) given by:

$$Q_{ij2} = \frac{4r_{sij}\left(T_i - T_j\right)}{\frac{1}{k_{si}} + \frac{1}{k_{sj}}} \tag{3.55}$$

Model B:

This model assumes that each pebble has an isothermal core of radius R_c with a representative temperature.

Case 1: The heat flux for the elementary volume of the bottom sphere shown in Figure 3.14 (b) is:

$$dQ_{ij} = 2\pi r^2 \sin\theta \, d\theta \left(-k_{si}\frac{dT}{dr}\right) \tag{3.56}$$

where dT/dr is the temperature profile in the radial direction. After integration of dT/dr and re-arranging the equations, the following is obtained:

$$dQ_{ij} = \frac{\left(T_i - T_j\right) d\theta}{\frac{\left(\frac{1}{R_c} - \frac{1}{R_p}\right)}{\left(2\pi k_{si}\sin\theta\right)} + \frac{\left(\frac{1}{R_p} - \frac{1}{R_\theta}\right)}{\left(\pi k_f \sin\theta\right)} + \frac{\left(\frac{1}{R_c} - \frac{1}{R_p}\right)}{\left(2\pi k_{sj}\sin\theta\right)}} \tag{3.57}$$

Integration of Eq. (3.57) yields the following:

$$Q_{ij} = \pi\left(T_i - T_j\right)\left(\frac{1}{b}\right)\ln\left(\frac{a - b\cos\theta_0}{a - b}\right) \tag{3.58}$$

where

$$a = \left(\frac{1}{2k_{si}} + \frac{1}{2k_{sj}}\right)\left(\frac{1}{R_c} - \frac{1}{R_p}\right) + \frac{1}{k_f R_p} \tag{3.59}$$

$$b = \frac{1}{k_f\left(R_p + h\right)} \tag{3.60}$$

$$\cos\theta_0 = \frac{R_p + h}{\sqrt{\left(R_p + h\right)^2 + R_{ij}^2}} \tag{3.61}$$

Case 2: The heat flux Q_{ij} is again the sum of Q_{ij1}, the conductivity through the solid spheres and stagnant fluid in between, and Q_{ij2} the conduction through the contact area between spheres. Similar to Case 1 but with one changed boundary condition, Q_{ij1} is given by:

$$Q_{ij1} = \pi\left(T_i - T_j\right)\left(\frac{1}{b}\right)\ln\left(\frac{a - b\cos\theta_0}{a - b\cos\theta_c}\right) \tag{3.62}$$

where

$$\cos\theta_c = \frac{R_p + h}{\sqrt{\left(R_p + h\right)^2 + r_{sij}^2}} \tag{3.63}$$

The heat flux through the contact surface area between two spheres Q_{ij2} can also be determined by Eq. (3.53). Finally, Cheng *et al.* (1999:4199) noted that conduction through the contact area between spheres plays an important role when $\kappa \geq 10^3$.

MODEL 10: Siu & Lee (2000:3917)

Siu & Lee (2000:3917) developed a semi-packing-structure-based method to calculate the effective thermal conductivity for the solid region of a packed bed. In their model much attention was given to characterise the packing structure through the coordination number and the contact angle using an analogy with structured packings. This method is therefore only valid for packed beds with porosities below 0.5 and where the thermal conductivity of the solid is much larger than that of the surrounding fluid matrix. Thus, in essence it is only valid to calculate the effective thermal conductivity of a packed bed under vacuum conditions.

They mention that most effective thermal conductivity models use empirical parameters and that these empirical models often assume a parallel heat flow to compute the effective thermal conductivity. However, this assumption begins to break down as the thermal conductivity of the solid fluid phases takes on different magnitudes. Therefore, Siu & Lee (2000:3917) developed a more flexible method to calculate the effective thermal conductivity in a randomly packed bed. They assumed a randomly packed bed, based on three different ordered structures, a SC, BCC or FCC (Figure 3.15). Thereafter, they assigned a certain porosity range to each of the aforementioned packing structures as shown in Table 3.2.

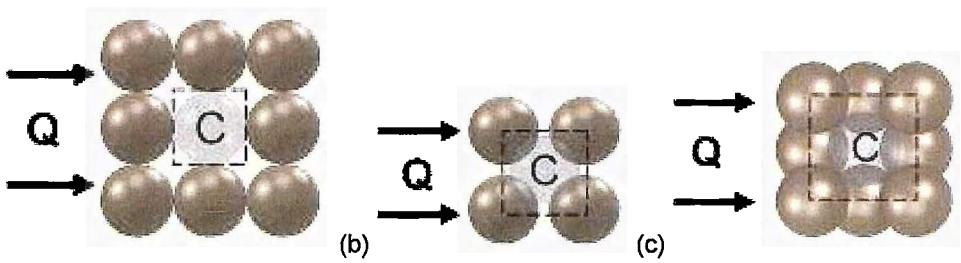

Figure 3.15: Sectional view showing the thermal path through sphere "C" in the (a) SC, (b) BCC and (c) FCC unit cells

In Table 3.2, the parameter N_A is defined as the number of spheres per unit area, N_L the number of spheres per unit length, with n the coordination flux number and N_c the coordination number. The effective thermal conductivity of each ordered unit cell can be computed from Fourier's Law given in Eq. (3.64), where Q is the total heat flux resulting from the driving potential of ΔT :

$$Q = k_e^{g,c} A \frac{\Delta T}{L} \Rightarrow k_c^{g,c} = \frac{L}{A} \frac{Q}{\Delta T} \tag{3.64}$$

Table 3.2: Suitable packing arrangements for different porosity range (Siu & Lee, 2000:3917)

TYPE OF ARRANGEMENT OF SPHERES	POROSITY RANGE[4]	N_A	N_L	n	$R(\beta)$	N_c
SC array	$\varepsilon: 0.35-0.5$	$\frac{1}{(4r_p^2)}$	$\frac{1}{(2r_p)}$	1	$R(180^o)$	6
BCC array	$\varepsilon: 0.2595-0.35$	$\frac{3}{(16r_p^2)}$	$\frac{\sqrt{3}}{(2r_p)}$	4	$R(70.53^o)$	8
FCC array	$\varepsilon \leq 0.2595$	$\frac{1}{(4r_p^2)}$	$\frac{1}{(\sqrt{2}r_p)}$	4	$R(90^o)$	12

Invoking the definition of thermal resistance, the effective thermal conductivity can be defined by Eq. (3.65), where L and A are the length and cross-sectional area of the unit cell, while R is the total thermal resistance imposed by the unit cell:

$$k_e^{g,c} = \frac{L}{A}\frac{1}{R} \tag{3.65}$$

The total resistance of the unit cell is the sum of the resistances within and between the spheres (sphere and contact resistance), neglecting thermal conductivity through the fluid and any resistance that may occur owing to pebble surface roughness. Therefore, the total thermal resistance R is dependent on the total thermal path, which is different for various packing structures.

Schematics of SC, BCC and FCC unit cells are shown in Figure 3.16, subjected to a uni-directional heat flow Q. Siu & Lee (2000:3920) defined heat flow angles for the various packings. For the SC packing, the heat passes from the left sphere to the right sphere through sphere C, resulting in one thermal path of 180° formed by the three spheres (Figure 3.16 (a)). In contrast, the BCC and FCC unit cells shown in Figure 3.16 (b) and Figure 3.16 (c) contain four parallel thermal paths through sphere C, with respective orientations of 70.53° and 90°. Thus, R_s is denoted as the resistance of one thermal path with an orientation of β. The resistance R_s for a SC unit cell imposed by sphere C is $R(180)$, and for BCC and FCC unit cells are $R(70.53)/4$ and $R(90)/4$ respectively. The total resistance for mono-sized spheres in general can vary from $60^o \leq \beta \leq 180^o$ and is given by:

[4] Siu & Lee (2000:3919) presented in Table 1 that the range of a BCC packing is from 0.25 to 0.3. This range, however, is extended to 0.25 to 0.35, in order to cover the whole porosity range to where $\varepsilon < 0.5$. The same was done for a FCC packing.

$$R_s = \frac{R(\beta)}{n} \tag{3.66}$$

Siu & Lee (2000:3920) also defined a total thermal resistance for a packed bed by assuming a number of spheres connected in parallel and series, which is given as follows:

$$k_e^{g,c} = \frac{N_A}{N_L}\frac{n}{R(\beta)} \tag{3.67}$$

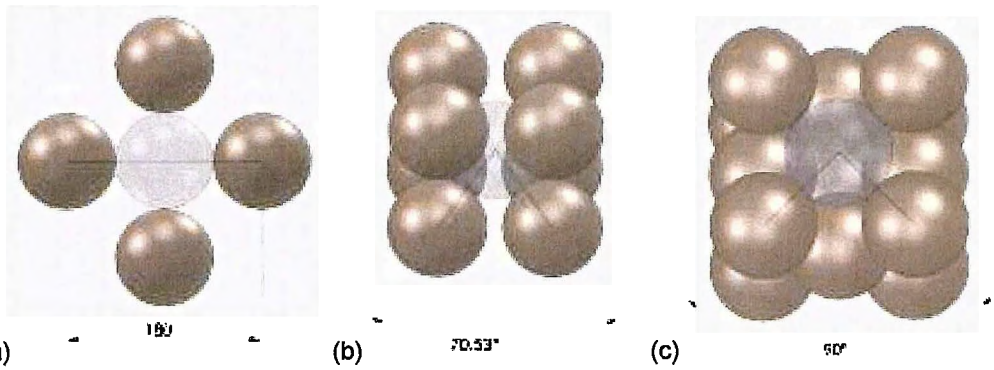

(a) (b) (c)

Figure 3.16: Schematic showing the angle of the thermal path in the (a) SC, (b) BCC and (c) FCC unit cells

Numerical calculations (CFD) were used to solve the resistance values $R(\beta)$ for various sphere sizes r_p, contact radius ratios $\gamma = r_c/r_p$ and contact angles β, and stated a validity for the correlation of $60° \le \beta \le 180°$, noting a minor discrepancy when $\beta = 60°$. The empirical correlation is then given by:

$$R(\beta) = R(180) + \left[0.64\sin^2\left(\frac{\beta}{2}\right) - 0.08\sin\left(\frac{\beta}{2}\right) - 0.56\right](k_s r_p) \tag{3.68}$$

with

$$R(180) = \frac{0.54038}{k_s r_p \gamma}\left[1 + 1.92069\gamma - 9.18530\gamma^2 + 17.5257\gamma^3\right] \tag{3.69}$$

where γ was obtained by a relation between contact area ratio and deformation ratio χ.

MODEL 11: Slavin et al. (2002:4151)

Slavin *et al.* (2002:4151) presented a model to calculate the effective thermal conductivity by including a measurable parameter for pebble roughness. With this, the thermal conductivity for an uncompressed bed can be calculated with no adjustable parameters, provided that the thermal conductivity of the solid is much larger than the fluid phase and gas pressures are above 4 kPa.

The model presented below was originally derived for sphere diameters in the range of 1 mm to 3 mm. Much attention was given to the Knudsen regime to incorporate the Smoluchowski effect (Section 3.1) with such small spheres.

Slavin *et al.* (2002:4151) noted that the bulk porosity of a randomly packed bed can vary between 0.35 and 0.43, whereas a SC packing yields a porosity of 0.476 and FCC packings 0.2595. They argued that 50% of the spheres in a randomly packed bed would not be in a FCC packing.

For that assumption, they derived a model to calculate the volume of a unit cell with two separable fractions: one where spheres are in a FCC arrangement and one where deviations from the FCC packing have left larger voids as displayed in Figure 3.17. The volume of the overall unit cell is therefore given by:

$$V = A_{cp}L + A_v L \tag{3.70}$$

where $A_{cp} = 2\sqrt{3}r_p^2$, $A_v = \left(\left(\sqrt{2/3}\pi/(1-\varepsilon)\right) - 2\sqrt{3}\right)r_p^2$, $L = \sqrt{8/3}r_p$.

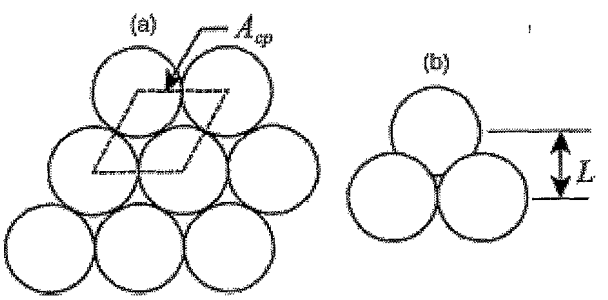

Figure 3.17: Unit cell in the FCC fraction (a) top view and (b) side view (Slavin et al., 2002:4151)

The average height of the surface roughness is denoted as h_r. The contact points between two spheres are separated by a short cylinder of area δ and length/height $2h_r$. This is displayed schematically in Figure 3.18, where r_p is the sphere radius and θ_λ, the polar angle at which $2/3\lambda = 2h_r$, with λ the molecular mean free path of the gas. Slavin *et al.* (2002:4151) note that the average distance that a gas molecule travels perpendicular to a surface before colliding with another molecule is $2/3\lambda$. The mean free path is given by:

$$\lambda = \frac{kT}{\sqrt{2}\pi p_g D_m^2} \tag{3.71}$$

where the Knudsen number is $Kn = \lambda/d$, D_m is the molecular diameter, p_g is the gas pressure, T is the temperature, k is the Boltzmann constant 1.3806505×10^{-23} $[J\cdot K^{-1}]$, and

d is the geometrical gas gap between surfaces that can be equal to $2h_r$. Knowing the mean free path the following can be derived for when $2/3\lambda > 2h_r$:

$$\theta_\lambda = \left(\left(\frac{2}{3}\lambda - 2h_r\right)\Big/ r_p\right)^{\frac{1}{2}} \tag{3.72}$$

and

$$r_\lambda = \left(\left(\frac{2}{3}\lambda - 2h_r\right) r_p\right)^{\frac{1}{2}} \tag{3.73}$$

When $2/3\lambda \le 2h_r$ the Smoluchowski effect is not applicable and yields the following $\theta_\lambda = 0$ and $r_\lambda = 0$.

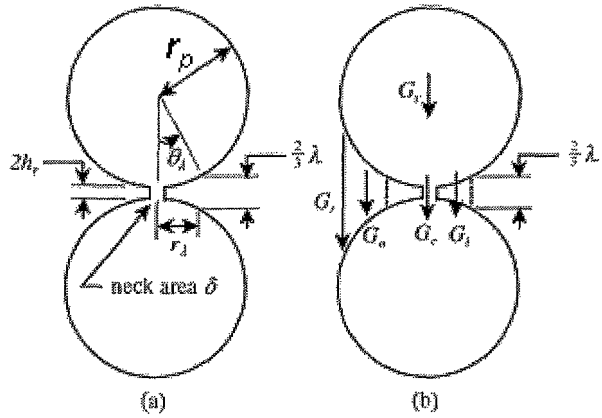

Figure 3.18: Model for two contacting spheres: (a) geometrical parameters (b) conductances
(Slavin *et al.*, 2002:4151)

The effective thermal conductivity of the unit cell can be defined if T_1 and T_2 are the temperatures at the top and bottom of the overall unit cell by:

$$\dot{Q} = K\left(A_{cp} + A_v\right)\frac{T_1 - T_2}{L} = G\left(T_1 - T_2\right) \tag{3.74}$$

where

$$G = G_{cp} + G_v \tag{3.75}$$

with

$$G_{cp} = \left[G_r + n\left(\frac{G_s\left(G_i + G_o + G_c\right)}{G_s + G_i + G_o + G_c}\right)\right] \tag{3.76}$$

$$G_v = \left(G_{rv} + G_{gv}\right) \tag{3.77}$$

As displayed in Figure 3.18, the heat flow will be represented by a number of conductances in series and parallel, where G_s is the conductance through the solid sphere and G_r is the

radiation between spheres. The gaseous thermal conduction is divided into two regions: an 'inner' region of radius r_λ, for which the gap between the two spheres is less than $2/3\lambda$, with a conductance G_i, and an 'outer' region, for which the gap is greater than $2/3\lambda$, with conductance G_o. The conductance through the physical contact of area δ is G_c. Additional conductances are also included in the void fraction of the bed: G_{rv} by radiation and G_{gv} by gaseous thermal conduction across the void. The expressions for the conductances are as follows:

$$G_s = \frac{\alpha_s k_s \pi r_p}{2} \tag{3.78}$$

$$G_c = \frac{\alpha_c k_s \delta}{2h_r} \tag{3.79}$$

$$G_r = \alpha_r \frac{4\sigma}{2/\varepsilon_r - 1} A_{cp} T^3 \tag{3.80}$$

$$G_i = \frac{a_T}{2-a_T} \frac{\gamma+1}{8} n_m \bar{v} C_v \pi r_\lambda^2 \tag{3.81}$$

$$G_o = K_o \pi R^2 \left(1 - e^{-R/\lambda}\right) \left\{ \begin{array}{l} \dfrac{\left(\cos\theta_{\max} - \cos\theta_\lambda\right)}{R} \\ + \dfrac{R + j + h_r}{R^2} \left[\begin{array}{l} \ln\left(R - R\cos\theta_{\max} + j + h_r\right) \\ -\ln\left(R - R\cos\theta_\lambda + j + h_r\right) \end{array} \right] \end{array} \right\} \tag{3.82}$$

$$G_{rv} = \alpha_r \frac{4\sigma}{2/\varepsilon_r - 1} A_v T^3 \tag{3.83}$$

$$G_{gv} = K_o \left(1 - \exp\left(\frac{-r_p}{\lambda}\right)\right) \frac{A_v}{L} \tag{3.84}$$

Here the α's are non-dimensional empirical constants and k_s is the thermal conductivity of the bulk solid material, n_m is the number of gas molecules per unit volume, a_T is the accommodation coefficient, $\gamma = C_p / C_v$ is the ratio of the gas heat capacities per molecule, and l is the gap length between spheres at the point of interest. The average molecular velocity is defined as $\bar{v} = \left(8kT/\pi M_g\right)^{1/2}$ where M_g is the molecular mass of the gas. Finally, a temperature jump parameter can be calculated with:

$$j = \left(\frac{2-a_T}{a_T}\right)\left(\frac{2\gamma}{(\gamma+1)}\right)\left(\frac{\gamma}{\mathrm{Pr}}\right) \tag{3.85}$$

where Pr is the Prandtl number. For helium the temperature jump is $j = 1.8\lambda$.

Slavin *et al.* (2002:4155) also brought the coordination flux number into consideration and defined an empirical constant α_s as $\alpha_s = 2/n$, assuming $n = 1.5$, the same assumption made by Kunii & Smith (1960:71). They also assumed a radiation view factor equal to 1 and defined $\alpha_r = 1$, which is only valid for relatively low temperatures. Furthermore, Slavin *et al.* (2002:4151) disregarded the contact thermal conduction and therefore did not assign a value to the correction factor α_c.

MODEL 12: Shapiro et al. (2004:268)

Shapiro *et al.* (2004:268) measured the effective thermal conductivity of ceramic powder packed beds at temperatures below 100°C for powder sizes smaller than 2.8 mm and compositions under different gas pressures. Using this experimental data, they developed a new model on the basis of the model proposed by Bauer & Schlünder (1978:189). In the Shapiro *et al.* (2004:268) model, the pebble bed is assumed to be composed of identical spheres with a contact area of πr_c^2 between adjacent spheres. It is further assumed that the heat is transferred through the gas and via each contact area. The model is simplified by assuming the spheres to be cylinders of radius d, height L, contact thickness δ and a contact area radius r_c, as displayed in Figure 3.19. The effective thermal conductivity is then given by:

$$k_e^{g,c} = \frac{4}{\pi} k_s \frac{1+\frac{\delta}{L}}{1+\left(\frac{\delta}{L\kappa_{sr_c}}\right)\left(\frac{1}{1-\alpha}\right)\left(\frac{1}{\kappa_{\delta r_c}}+\frac{1}{\alpha^{-1}-1}\right)^{-1}} \tag{3.86}$$

where $\alpha = 2r_c^2/d^2$, $\kappa_{sr_c} = k_{r_c}/k_s$, $\kappa_{\delta r_c} = k_{r_c}/k_\delta$.

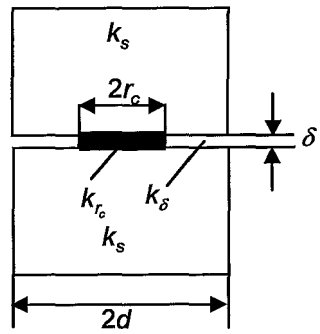

Figure 3.19: Schematic model of heat transfer through a contact area in a powder bed (Shapiro et al., 2004:269)

Shapiro *et al.* (2004:268) also accounted for the Smoluchowski effect by introducing a pressure dependent parameter into their model given by:

$$k_\delta = k_f \left[\frac{j}{p_g \delta} + 1 \right]^{-1} \tag{3.87}$$

with the modified temperature jump parameter given by:

$$j = \left(\frac{4\gamma}{\gamma + 1} \right) \left(\frac{2 - a_T}{a_T} \right) \frac{\lambda_0 P_0}{\mathrm{Pr}} \tag{3.88}$$

where $\gamma = \left(C_p / C_v\right)$ is the specific heat ratio of the gas, λ_0 is the mean free path at atmospheric pressure, Pr is the Prandtl number, a_T is the accommodation coefficient, k_f is the gas thermal conductivity at atmospheric pressure, p_g is the gas pressure, and P_0 is the atmospheric pressure. The values of the contact thickness δ and the contact area size r_c are selected empirically to obtain the best fit with experimental data.

3.2.2 EFFECTIVE THERMAL CONDUCTIVITY DUE TO CONTACT AREA

Contact area at high solid to fluid or gas thermal conductivity ratios $\kappa \geq 10^3$ is of significant importance as previously mentioned. Hsu *et al.* (1994:2751) stated that finite-area contacts between spheres are likely to occur in a packed bed of spheres due to external loads or their own weight.

One important fundamental distinction that may be made is that between contact area and pebble surface roughness. Contact area is defined as the contact region between two spheres, which increase in area with external load due to the elasticity of the solid material. Whereas pebble roughness is defined as small gaps between the contacts of two spheres that influence the heat transfer. This heat transfer is mainly influenced by the Smoluchowski effect where a reduction in conduction occurs through the small gas filled gaps. This section illustrates some models considering heat transfer through contact area, pebble roughness or both.

MODEL1: Bauer & Schlünder (1978:189)

This model, also referred to as the Zehner, Bauer, Schlünder (ZBS) model, is an extension of the work of Zehner & Schlünder (1970:933). Bauer & Schlünder (1978:189) improved the model of Zehner & Schlünder (1970:933) by including radiation, considering the Knudsen

regime (Smoluchowski effect) and introducing a surface fraction parameter φ for heat transfer through the contact area as displayed in Figure 3.20. The effective thermal conductivity $k_e^{g,c,r}$ can be calculated as follows:

$$\frac{k_e^{g,c,r}}{k_f} = \left(1-\sqrt{1-\varepsilon}\right)\varepsilon\left[\left(\varepsilon-1+\frac{1}{\kappa_G}\right)^{-1}+\kappa_r\right]+\sqrt{1-\varepsilon}\left[\varphi\kappa+(1-\varphi)k_c\right] \tag{3.89}$$

where

$$k_c = \frac{2}{N}\left\{\begin{aligned}&\frac{B(\kappa+\kappa_r-1)}{N^2\kappa_G\kappa}\ln\frac{\kappa+\kappa_r}{B\left[\kappa_G+(1-\kappa_G)(\kappa+\kappa_r)\right]}\\&+\frac{B+1}{2B}\left[\frac{\kappa_r}{\kappa_G}-B\left(1+\frac{1-\kappa_G}{\kappa_G}\kappa_r\right)\right]-\frac{B-1}{N\kappa_G}\end{aligned}\right\} \tag{3.90}$$

and

$$N = \frac{1}{\kappa_G}\left(1+\frac{\kappa_r-B\kappa_G}{\kappa}\right)-B\left(\frac{1}{\kappa_G}-1\right)\left(1+\frac{\kappa_r}{\kappa}\right) \tag{3.91}$$

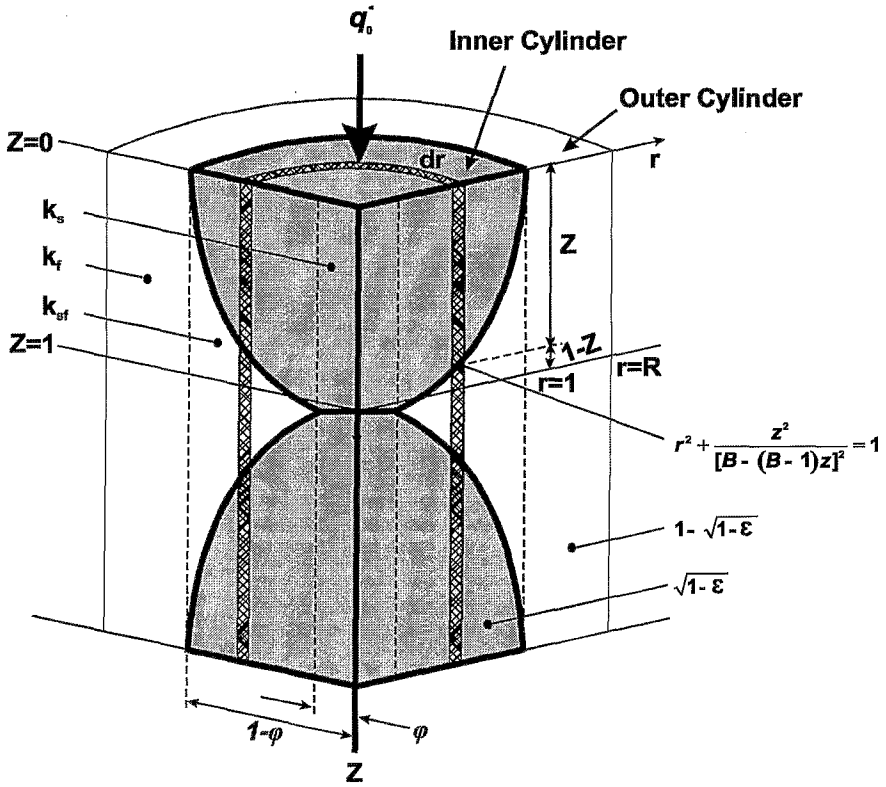

Figure 3.20: Bauer & Schlünder unit cell model with contact area (Bauer & Schlünder, 1978:189)

Again B is an approximated value that varies with porosity, where values for C and m are described in the paragraph following Eq. (3.22).

$$B = C\left(\frac{1-\varepsilon}{\varepsilon}\right)^m \tag{3.92}$$

The radiation parameter is given by:

$$\kappa_r = \frac{k_e^r}{k_f} = \frac{4\sigma}{\left(\frac{2}{\varepsilon_r}-1\right)} T^3 \frac{d_p}{k_f} \tag{3.93}$$

The gaseous thermal conduction is related to the Knudsen regime by:

$$\kappa_G = \frac{k_G}{k_f} = \left[1+\left(\frac{l}{d_p}\right)\right]^{-1} \tag{3.94}$$

where l is a modified free path of the gas molecules defined by:

$$l = 2\frac{2-a_T}{a_T}\left(\frac{2\pi\tilde{R}T}{M_g}\right)^{1/2} \cdot \frac{k_f}{p_g\left(2C_p - \tilde{R}/M_g\right)} \tag{3.95}$$

with T the absolute temperature in [K], p_g gas pressure [Pa], $\tilde{R}$ the universal gas constant, M_g the molecular mass of the gas, k_f the molecular thermal conductivity of the gas, k_G the thermal conductivity with variance in gas pressure, k_e^r the radiative thermal conductivity, and a_T the accommodation coefficient.

It is important to note that Bauer & Schlünder (1978:192) stated that the contact area fraction φ is a function of many undetermined limiting quantities, such as the elasticity of the material, the external mechanical stress and the surface state of the material. They also mentioned that contact area must be obtained experimentally.

MODEL 2: Hsu et al. (1994:2751)

Hsu *et al.* (1994:2751) questioned the model of Zehner & Schlünder (1970:933) at solid-to-fluid thermal conductivity ratios above $\kappa \geq 10^3$. They postulated that the reason the Zehner & Schlünder (1970:933) model under-predicts the stagnant thermal conductivity of a packed bed of spheres at high solid-to-fluid thermal conductivity ratios is that the model assumes point contacts between spheres rather than contact areas. Therefore, Hsu *et al.* (1994:2751) argued that the Zehner & Schlünder (1970:933) model could be improved by incorporating the effects of pebble-to-pebble contacts through a finite contact area.

The primary modification made to the Zehner & Schlünder (1970:933) model is the introduction of a flat region on the surface of the sphere occupying the unit cell (Figure 3.21).

Hsu *et al.* (1994:2751) modified Eq. (3.18) by introducing an empirical deformation factor α_0 accounting for the contact area.

Thus, changing the equation to:

$$r^2 + \frac{z^2}{\left[(1+\alpha_0)B-(B-1)z\right]^2} = 1 \tag{3.96}$$

When $\alpha_0 = 0$, Eq. (3.96) reduces to Eq. (3.18). The modified solid-to-fluid interface is illustrated in Figure 3.21, where r_s is the radius of the contact area that can be determined by imposing the condition $r = r_s, z = 1$. Substitution of these aforementioned conditions into Eq. (3.96) leads to:

$$r_s^2 = 1 - \frac{1}{(1+\alpha_0 B)^2} \tag{3.97}$$

The one-dimensional heat conduction in the unit cell consists of three parallel paths: the outer concentric cylinder consisting of the fluid phase, the middle concentric cylinder consisting of both the solid and fluid phases and the inner cylinder consisting of the solid phase. This leads to the effective stagnant thermal conductivity given by:

$$k_e^{g,c} = \left(1-\frac{1}{R^2}\right)k_f + \left(\frac{1-r_s^2}{R^2}\right)k_{fs} + \left(\frac{r_s}{R}\right)^2 k_s \tag{3.98}$$

where R is a function of porosity. The resulting effective thermal conductivity of the unit cell is then given by:

$$\begin{aligned}\frac{k_e^{g,c}}{k_f} = {} & \left[1-\sqrt{(1-\varepsilon)}\right] + \frac{\sqrt{(1-\varepsilon)}}{\kappa^{-1}}\left(1-\frac{1}{(1+\alpha_0 B)^2}\right) \\ & + \frac{2\sqrt{(1-\varepsilon)}}{\left[1-\kappa^{-1}B+\left(1-\kappa^{-1}\right)\alpha_0 B\right]}\left(\begin{array}{l}\dfrac{\left(1-\kappa^{-1}\right)(1+\alpha_0)B}{\left[1-\kappa^{-1}B+\left(1-\kappa^{-1}\right)\alpha_0 B\right]^2} \\ \times \ln\left(\dfrac{1+\alpha_0 B}{(1+\alpha_0)B\kappa^{-1}}\right) - \dfrac{B+1+2\alpha_0 B}{2(1+\alpha_0 B)^2} \\ - \dfrac{(B-1)}{\left[1-\kappa^{-1}B+\left(1-\kappa^{-1}\right)\alpha_0 B\right](1+\alpha B)}\end{array}\right)\end{aligned} \tag{3.99}$$

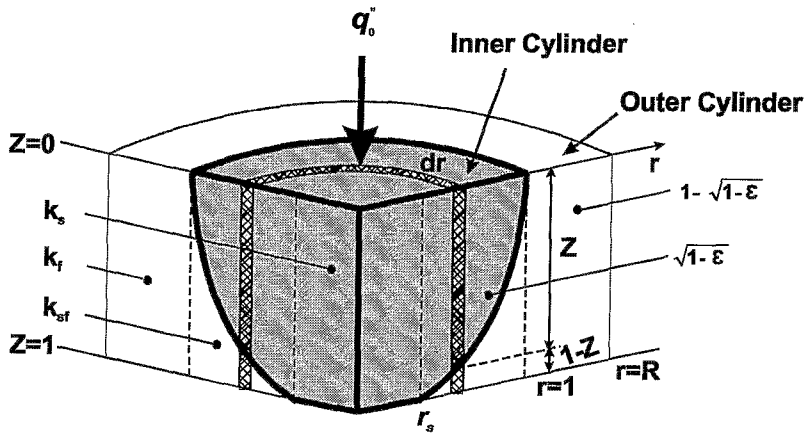

Figure 3.21: Hsu et al. modifications to the Zehner & Schlünder unit cell (Hsu et al., 1994:2751; Zehner & Schlünder, 1970:933)

The introduction of the contact parameter causes the geometric parameter B in Eq. (3.99) to become a function of α_0. Consequently, B is determined from:

$$\varepsilon = 1 - \frac{B^2}{(1-B)^6(1+\alpha_0 B)^2}\left[\begin{array}{l}(B^2-4B+3)+2(1+\alpha_0)(1+\alpha_0 B)\\ \times\ln\left(\frac{(1+\alpha_0)B}{1+\alpha_0 B}\right)+\alpha_0(B-1)(B^2-2B-1)\end{array}\right]^2 \tag{3.100}$$

Hsu *et al.* (1994:2755) found that $\alpha_0 = 0.002$ and $\varepsilon = 0.42$ yields the best agreement with data obtained from Nozad *et al.* (1985b:857).

MODEL 3: Kaviany (1991:127)

Kaviany (1991:127) presented a model that calculates the contact area between two spheres, using Hertzian elastic deformation principles. The radius of the contact area r_c between two spheres of radius r_p can be calculated by using the Poisson ratio μ_p, the Young modules E_p and a collinear force F acting on the pebble.

$$r_c = \left[\frac{3(1-\mu_p^2)}{4E_p}Fr_p\right]^{\frac{1}{3}} \tag{3.101}$$

Kaviany (1991:127) then presented the overall conductance due to the contact area. This is achieved by assuming that a randomly packed bed can be quantified using ordered packings.

$$\frac{k_e^c}{k_s} = \left[\frac{3(1-\mu_p^2)}{4E_p}Fr_p\right]^{\frac{1}{3}}\frac{1}{0.531S}\left(\frac{N_A}{N_L}\right) \tag{3.102}$$

where the force F [N] is related to the external pressure p_F [Pa] through:

$$F = p_F \frac{S_F}{N_A} \tag{3.103}$$

with N_A and N_L the number of spheres per unit area and length respectively (Table 3.2). The constants S and S_F are given in Table 3.3. It should, however, be noted that certain porosity ranges are not defined in Table 3.3 and is taken to be the same as those displayed in Table 3.2 in calculations.

Table 3.3: Magnitude of structural parameters for different close packings of spheres (Kaviany, 1991:129)

TYPE OF ARRANGEMENT OF SPHERES	POROSITY RANGE	S	S_F
SC array	ε: 0.5 – 0.35	1	1
BCC array	ε: 0.3 – 0.25	0.25	$\frac{\sqrt{3}}{4}$
FCC array	$\varepsilon \leq 0.2$	$\frac{1}{3}$	$\frac{1}{\sqrt{6}}$

MODEL 4: Bahrami et al. (2006:3691)

Bahrami *et al.* (2006:3691) developed a new compact resistance model that predicts the effective thermal conductivity of randomly packed beds with rough, mono-sized spheres immersed in a stagnant gas at various gas pressures (from atmospheric to vacuum) and subjected to a range of mechanical loads. Bahrami *et al.* (2006:3691) focused on three heat transfer paths: the interstitial gas within the microgap Q_g, microcontacts Q_s and the interstitial gas within the macrogap Q_G, as displayed in Figure 3.22.

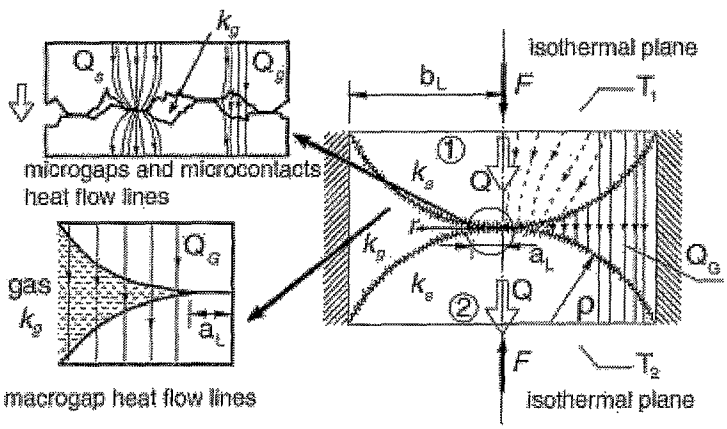

Figure 3.22: Contact of rough spheres with presence of interstitial gas (Bahrami et al., 2006:3693)

The thermal contact resistance of the rough spherical surfaces with the presence of an interstitial gas contains four thermal resistance components: the macrocontact constriction/spreading resistance R_L, the microcontacts constriction/spreading resistance R_s, the resistance of the interstitial gas in the microgap R_g, and the resistance of interstitial gas in the macrogap R_G, see Figure 3.23.

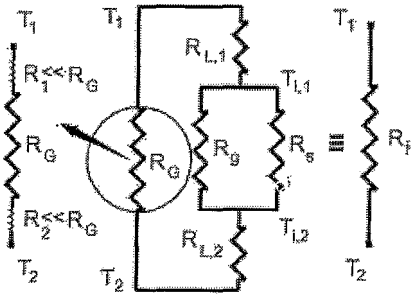

Figure 3.23: Thermal resistance network, spherical rough contacts in presence of gas (Bahrami et al., 2006:3693)

The macrogap provides a parallel path for conduction between the two isothermal planes (gas/solid), therefore the contact resistance between two spheres can be calculated from:

$$R_j = \left[\frac{1}{\left(1/R_s + 1/R_g\right)^{-1} + R_L} + \frac{1}{R_G} \right]^{-1} \tag{3.104}$$

It is important to note that R_G has three components: the macrogap resistance and the bulk thermal resistance of the solid layers in sphere 1 and 2 (R_1 and R_2), respectively. However, Bahrami *et al.* (2006:3693) stated that R_1 and R_2 are negligible compared to R_G, as the gas thermal conductivity is much smaller than the thermal conductivity of the solids, that is large κ values. This is, however, not the case when $\kappa \approx 1$ and has not been investigated by Bahrami *et al.* (2006:3693).

Microcontacts thermal resistance R_s

The thermal constriction/spreading resistance through the microcontacts R_s, assuming plastically deformed asperities are derived as follows:

$$R_s = \frac{0.565 H^* \left(\frac{\sigma_{RMS}}{m_{RMS}} \right)}{k_s F} \tag{3.105}$$

where

$$k_s = 2k_{s1}k_{s2} / \left(k_{s1} + k_{s2}\right) \tag{3.106}$$

$$H^* = c_1\left(\sigma' / m_{RMS}\right)^{c_2} \tag{3.107}$$

$$\sigma' = \sigma_{RMS} / \sigma_0 \text{ with } \sigma_0 = 1\mu m \tag{3.108}$$

and the coefficients for Vickers microhardness:

$$c_1 = H_{BGM}\left(4.0 - 5.77\kappa_c + 4.0\kappa_c^2 - 0.61\kappa_c^3\right) \tag{3.109}$$

$$c_2 = -0.57 + 0.82\kappa_c - 0.41\kappa_c^2 + 0.06\kappa_c^3 \tag{3.110}$$

where $\kappa_c = H_B / H_{BGM}$, H_B is the Brinell hardness of the bulk material in GPa and $H_{BGM} = 3.178\,GPa$. The above correlations are valid for the range $1.3 \le H_B \le 7.6\,GPa$. In situations in which an effective value of microhardness H_{mic} is known, the Vickers microhardness coefficients will be $c_1 = H_{mic}$ and $c_2 = 0$. The combined Root Mean Square (RMS) roughness σ_{RMS} and surface slope m_{RMS} are displayed in Figure 3.24 and calculated as follows:

$$\sigma_{RMS} = \sqrt{\sigma_1^2 + \sigma_2^2}\ ,\ m_{RMS} = \sqrt{m_1^2 + m_2^2} \tag{3.111}$$

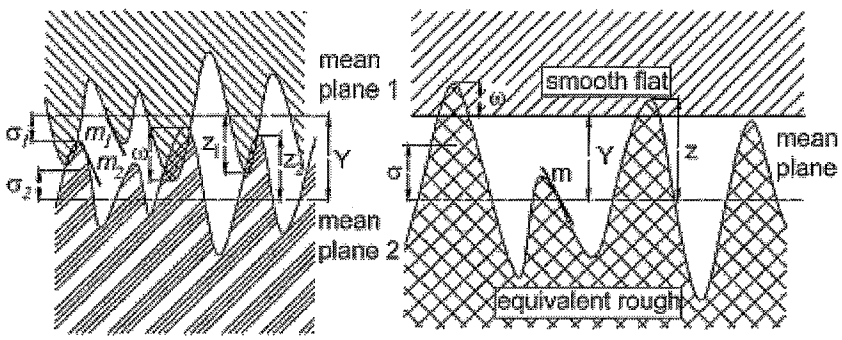

(a) Section through two contacting surfaces

(b) Corresponding section through equivalent rough-smooth flat

Figure 3.24: Schematic of pebble roughness and slope (Bahrami *et al.*, 2006:3)

Summarised in Table 3.4 are the correlations proposed by various researchers to obtain the relation between surface slope m and surface roughness σ. However, Bahrami *et al.* (2006:2) explicitly stated that the uncertainty of these correlations is high and should only be used when the surface slope is not reported and/or a rough estimate of m is needed.

Table 3.4: Correlations for m, Gaussian surfaces (Bahrami et al., 2006:2)

REFERENCE: (as quoted by Bahrami *et al.*, 2006:2)	CORRELATION $\sigma(m)$
Tanner & Fahoum (1976:299)	$m = 0.152\left(\sigma \cdot 10^6\right)^{0.4}$
Antonetti *et al.* (1991:35)	$m = 0.124\left(\sigma \cdot 10^6\right)^{0.743}, \sigma \le 1.6\mu m$
Lambert & Fletcher (1997:684)	$m = 0.076\left(\sigma \cdot 10^6\right)^{0.52}$

Macrocontact thermal resistance, R_L

Bahrami *et al.* (2006:3691) also proposed a general contact pressure distribution that covers the entire range of spherical rough contacts. This model also covers the limiting case of contact of smooth spheres (Hertzian contact). The following relationships were developed for the maximum contact pressure $P_{0,c}$ and the contact area radius a_L.

$$P_0' = \frac{P_{0,c}}{P_{0,H}} = \frac{1}{1+1.22\alpha\kappa_p^{-0.16}} \tag{3.112}$$

$$\frac{a_L}{a_H} = \begin{cases} \dfrac{1.605}{\sqrt{P_0'}}, & 0.01 \le P_0' \le 0.47 \\ 3.51 - 2.51P_0', & 0.47 \le P_0' \le 1 \end{cases} \tag{3.113}$$

where

$$P_{0,H} = \frac{1.5F}{\pi a_H^2} \tag{3.114}$$

The non-dimensional parameters α and κ_p can be obtained from Eq. (3.118), where the effective modulus of elasticity E_p', the equivalent radius of curvature $r_{p,eq}$ and the Hertzian contact radius a_H can be derived from:

$$\frac{1}{E_p'} = \frac{\left(1-\mu_{p1}^2\right)}{E_{p1}} + \frac{\left(1-\mu_{p2}^2\right)}{E_{p2}} \tag{3.115}$$

$$\frac{1}{r_{p,eq}} = \frac{1}{r_{p1}} + \frac{1}{r_{p2}} \tag{3.116}$$

Figure 3.25 details the procedure, which has been widely used for the geometric modelling of the actual contact between two curved rough bodies. As a result, the complex geometry of two curved shaped rough contacts is simplified to a contact between an equivalent truncated spherical surface and an equivalent rough flat surface (Bahrami *et al.*, 2006:3). It is important

to note that $r_{p,eq} = r_p$ when the joint resistance between a sphere and flat surface is calculated. The Hertzian contact radius is calculated by:

$$a_H = \left(\frac{3Fr_{p,eq}}{4E'_p} \right)^{\frac{1}{3}} \tag{3.117}$$

where $a_H = r_c$ in Eq. (3.101). The non-dimensional parameters α and κ_p are defined as:

$$\alpha = \frac{\sigma_{RMS} r_{p,eq}}{a_H^2} \text{ and } \kappa_p = \frac{E'_p}{H_{mic}} \sqrt{\frac{r_{p,eq}}{\sigma_{RMS}}} \tag{3.118}$$

Furthermore, Bahrami *et al.* (2006:3691) assumed that the macrocontact region is isothermal. Therefore, the macrocontact constriction/spreading resistance is given by:

$$R_L = \frac{1}{2k_s a_L} \tag{3.119}$$

where a_L is calculated using Eq. (3.113).

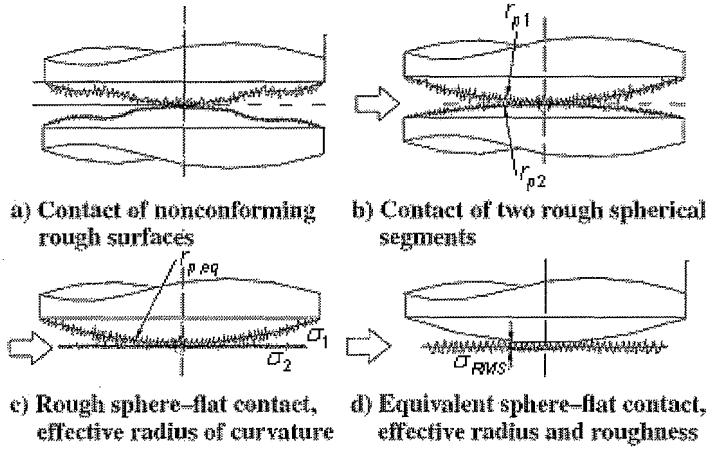

Figure 3.25: Summary of geometrical modelling (Bahrami et al., 2006:3)

Conduction through gas, R_g and R_G

In the microgap, Bahrami *et al.* (2006:3691) also took the Smoluchowski effect into account, with the Knudsen number. They demonstrated that the heat transfer in the Knudsen regime could effectively be calculated using a temperature jump distance j, which is defined as[5]:

[5] Bahrami *et al.* (2006:3694) note that the variable m in many cases should be a M. However, in this study M is denoted as j representing the temperature jump coefficient.

$$j = \left(\frac{2-a_{T1}}{a_{T1}} + \frac{2-a_{T2}}{a_{T2}}\right)\left(\frac{2\gamma}{1+\gamma}\right)\frac{1}{\mathrm{Pr}}\lambda \tag{3.120}$$

where $a_{T1}, a_{T2}, \gamma = C_p/C_v$ and Pr are thermal accommodation coefficients corresponding to the gas-solid combination of surface 1 and 2, ratio of the gas specific heats and the gas Prandtl number, respectively. The proposed correlation to estimate a_T for engineering surfaces 1 and 2 is given by:

$$a_T = \exp\left[-0.57\left(\frac{T_s - T_0}{T_0}\right)\right]\left(\frac{M_g^*}{6.8 + M_g^*}\right) + \frac{2.4\mu_m}{(1+\mu_m)^2}\left\{1 - \exp\left[-0.57\left(\frac{T_s - T_0}{T_0}\right)\right]\right\} \tag{3.121}$$

where

$$M_g^* = \begin{cases} M_g & \textit{for monatomic gases} \\ 1.4M_g & \textit{for diatomic / polyatomic gases} \end{cases} \tag{3.122}$$

where $T_0 = 273\,K$, T_s is the solid/sphere temperature, and $\mu_m = M_g/M_s$, with M_g and M_s the molecular mass of the gas and the solid, respectively. The microgap and the macrogap resistances for the contact between two rough spheres can be calculated from:

$$R_g = \frac{2\sqrt{2}\sigma_{RMS}a_2}{\pi k_g a_L^2 \ln\left(1 + \dfrac{a_2}{a_1 + \left(j/2\sqrt{2}\sigma_{RMS}\right)}\right)} \tag{3.123}$$

where

$$a_1 = erfc^{-1}\left(\frac{2P_{0,c}}{H'}\right),\quad a_2 = erfc^{-1}\left(\frac{0.03P_{0,c}}{H'}\right) - a_1 \tag{3.124}$$

The inverse complementary error function $erfc^{-1}(x)$ can be calculated from:

$$erfc^{-1}(x) = \begin{cases} \dfrac{1}{0.218 + 0.735x^{0.173}} & 10^{-9} \le x \le 0.02 \\ \dfrac{1.05(0.175)^x}{x^{0.12}} & 0.02 < x \le 0.5 \\ \dfrac{1-x}{0.707 + 0.862x - 0.431x^2} & 0.5 < x \le 1.9 \end{cases} \tag{3.125}$$

The resistance for the macrogap can be calculated as follows:

$$R_G = \frac{2}{\pi k_g \left[S \ln\left(\frac{S-B}{S-A}\right) + B - A \right]} \tag{3.126}$$

where

$$A = 2\sqrt{r_{p,eq}^2 - a_L^2}\ ,\ B = 2\sqrt{r_{p,eq}^2 - b_L^2} \tag{3.127}$$

and

$$S = r_{p,eq} - \omega_0 + j\ ,\ H' = c_1 \left(\frac{1.62\sigma'}{m}\right)^{c_2}\ ,\ \omega_0 = \frac{a_L^2}{2r_{p,eq}} \tag{3.128}$$

where $b_L = r_p$ for spheres.

3.2.3 EFFECTIVE THERMAL CONDUCTIVITY DUE TO RADIATION

Before discussing correlations predicting/representing radiative heat transfer in porous media, a discussion of radiative principles in packed beds is required. Figure 3.26 and Figure 3.27 give several general radiative properties, for which the following general definitions are required:

Diffuse surface: A surface for which the intensity of the emitted radiation is independent of direction, displayed in Figure 3.26 (a), (Incropera & De Witt, 2002:706).

Specular surface: Is the perfect, mirror-like reflection of light from a surface in which light from a single incoming direction (a ray) is reflected into a single outgoing direction, as displayed in Figure 3.26 (b) (www.answers.com).

Opaque: If attenuation is complete so that no penetration re-emerges (Modest, 1993:5). Therefore, no transmittance.

Gray surface: Defined as one for which absorptivity α and emissivity ε_r are independent of radiation wavelength λ over the spectral regions of the irradiation and the surface emission (Incropera & De Witt, 2002:741). Therefore, $\alpha = \varepsilon_r$.

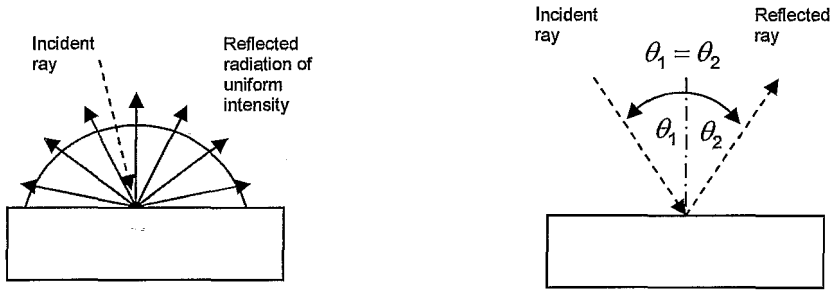

(a) Diffuse surface (b) Specular surface

Figure 3.26: Diffuse and specular reflection (Incropera & De Witt, 2002:733)

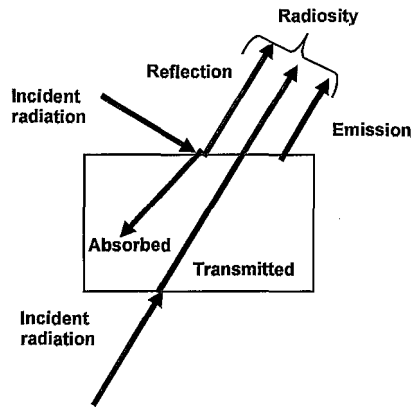

Figure 3.27: Radiation principles (Incropera & De Witt, 2002:711)

Lee *et al.* (2001:106) noted that over time many different methods to simulate radiative heat transfer in packed sphere systems have been developed. These methods can be grouped into the following three approaches:

Radiative transfer equation

The first approach is that of the Radiative Transfer Equation (RTE). The RTE approach is a radiative energy balance equation for the emitting, absorbing and scattering medium. However, in order to solve for the intensity distribution in a packing under consideration, a set of optical properties, such as scattering coefficient, absorption coefficient and phase function, must be obtained prior to the energy computation (Lee *et al.*, 2001:106). Each set of packed sphere systems require their own set of optical properties owing to the different microstructure of each packing. These optical properties can be obtained either experimentally or numerically. Argento & Bouvard (1996:3176) explained the RTE by considering the Two-flux Model, where results will be shown later on.

Unit cells

The second approach is that of the unit cell method. The unit cell approach makes use of

repeated units of idealised geometry, with the optical properties predetermined. Thus, the energy distribution for the system can be formulated into a set of simple algebraic equations (Lee *et al.,* 2001:106). The general form for the so-called "radiative thermal conductivity" for a unit cell in a PBR is defined as:

$$k_e^r = 4F_E^* \sigma d_p \overline{T}^3 \tag{3.129}$$

where F_E^* is defined as a radiation exchange factor, σ is the Stefan–Boltzmann constant and d_p is the pebble diameter. Strieder (1997:172) stated that the radiative thermal conductivity only retains validity on condition that it is assumed that the steady-state temperature drop ΔT across the local average bed dimension is much smaller than the average bed temperature $\overline{T}$, that is $\Delta T/\overline{T} = 1$. This is because most unit cell models make use of the averaging assumption that $\left(T_1^4 - T_2^4\right)/\left(T_1 - T_2\right) \approx 4\overline{T}^3$. Early attempts to define the radiation exchange factor were by Kasparek & Vortmeyer (1976:117), who defined the radiation exchange factor as a function of $F_E = f\left(\varepsilon, \varepsilon_r\right)$. However, Singh & Kaviany (1994:2579) demonstrated that the radiant thermal conductivity is strongly influenced by the solid thermal conductivity k_s and pebble emissivity ε_r, resulting in the radiation exchange factor to be a function of $F_E^* = f\left(\Lambda_s, \varepsilon, \varepsilon_r\right)$ with the dimensionless solid thermal conductivity as $\Lambda_s = k_s/4d_p\sigma T^3$. The most important limitation of the radiation exchange factor is that the value of F_E or F_E^* cannot be calculated easily. For this reason, Howell (2005:693) stated that many researchers recognised the inaccuracy of this simple approach.

However, although the unit cell approach can provide a set of fine-resolution solutions, the use of regularly structured units restricts the analysis of complex packed sphere structures (Lee *et al.,* 2001:106). This is noted when calculating the effective thermal conductivity at the near-wall interface where the porosity and packing structure changes.

Radiative transfer coefficient

The third approach is that of the Radiative Transfer Coefficient (RTC), which was developed by Lee *et al.* (2001:106). The RTC is a numerical method that can provide temperature solutions as fine as the size of the spheres. The RTC is a function of the microstructure (coordination number, area of contact and the distance between spheres centres) and radiative properties (reflectivity of sphere surface) of the packed sphere system. In the RTC approach, a set of algebraic equations is first established to compute the energy in each sphere. With the energy distribution known, the temperature for each sphere can be computed accordingly. The RTC is calculated using a Monte Carlo ray-tracing method. With the known RTC, the set of algebraic equations can be computed with an iterative scheme.

MODEL 1: Kunii & Smith (1960:71), and Yagi & Kunii (1957:373)

The model presented below is the result of the addition of radiation to Model 2 presented in Section 3.2.1. The same lumped parameter representation in Figure 3.5 accounts for this model for which the following equations were expressly derived:

$$\frac{k_{eff}}{k_f} = \varepsilon\left[1+\frac{\beta k_{rv} d_p}{k_f}\right] + \frac{\beta(1+\varepsilon)}{\left[\dfrac{1}{1/\psi_t + k_{rs} d_p/k_f} + \dfrac{\gamma}{\kappa}\right]} \tag{3.130}$$

where k_{rs} and k_{rv} are the radiation from solid to solid and void to void, respectively. As previously mentioned, Kunii & Smith (1960:72) concluded that $\gamma = 2/3$ and ψ_t is defined in the same manner as in Eq. (3.10).

$$k_{rs} = 0.1952\left[\frac{\varepsilon_r}{(2-\varepsilon_r)}\right]\left[\frac{T}{100}\right]^3 \approx 4\sigma T^3\left[\frac{\varepsilon_r}{(2-\varepsilon_r)}\right] \tag{3.131}$$

$$k_{rv} = \left[\frac{0.1952}{1+\dfrac{\varepsilon}{2(1-\varepsilon)}\dfrac{1-\varepsilon_r}{\varepsilon_r}}\right]\left[\frac{T}{100}\right]^3 \approx \left[\frac{4\sigma T^3}{1+\dfrac{\varepsilon}{2(1-\varepsilon)}\dfrac{(1-\varepsilon_r)}{\varepsilon_r}}\right] \tag{3.132}$$

It should be noted that the temperature T is in Kelvin.

MODEL 2: Chen & Churchill (1963:35)

Chen & Churchill (1963:35) obtained experimental results through investigating the effective scattering b and the absorption cross sections a. This was achieved by investigating the radiative transmission through isothermal beds filled with glass, aluminium oxide, steel spheres, cylinders and irregular grains, with the pebble diameter ranging between 3 mm and 5 mm. An example for 5 mm glass spheres is shown in Figure 3.28.

Consequently, Chen & Churchill (1963:35) developed a model treating the radiative heat transfer as a diffusion process, thus the radiative conductivity can be calculated from:

$$k_e^r = \frac{8\sigma T^3}{a+2b} \tag{3.133}$$

Argento & Bouvard (1996:3176) noted that the absorption and scattering coefficients are dependent on the geometry of the packing, spheres and the emissivity on the pebble surface. Consequently, they noted that the absorption and scattering coefficients do not depend on temperature, assuming that emissivity is independent of temperature. Therefore, they reworked the Chen & Churchill (1963:35) model and presented a dimensionless radiation

exchange factor:

$$F_E = \frac{2}{d_p(a+2b)} \tag{3.134}$$

where the radiant thermal conductivity is defined in Eq. (3.129). Despite the extensive research conducted by Chen & Churchill (1963:35), Cheng *et al.* (2002:1) stated that this model could not be used in general because the absorption and scattering coefficients are specific to the packing structure.

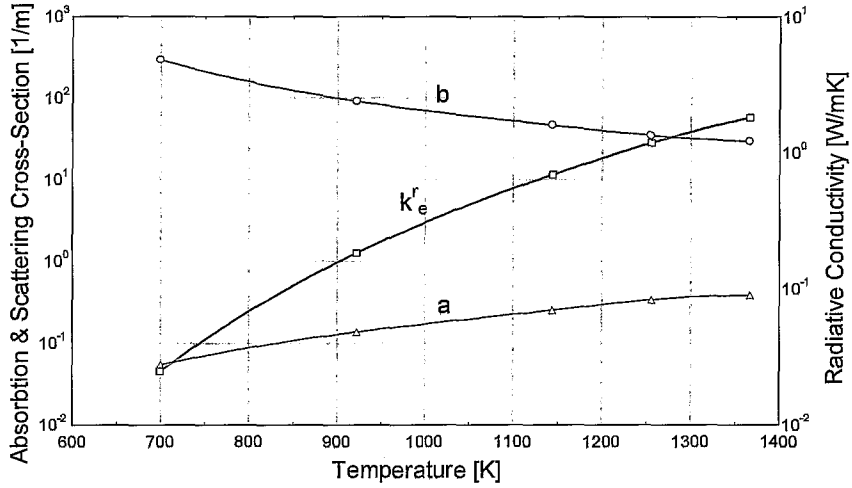

Figure 3.28: Radiant properties of a packed bed of 5 mm glass spheres (Chen & Churchill, 1963:35)

MODEL 3: Vortmeyer (1966:1)

Vortmeyer (1966:1) developed a one-dimensional radiation heat transfer model, in which the pebble bed is represented by a system of parallel layers of spheres perpendicular to the direction of heat flux. The layers can also exchange radiation through voids, causing an interaction between distant layers. The net heat flux is specified as follows:

$$q_i = I_i - K_i \tag{3.135}$$

where I_i and K_i are the forward and backward radiation flux respectively (Figure 3.29). Therefore, the following system of equations holds:

$$I_i = B \cdot I_{i-1} + R \cdot K_i + E_i \tag{3.136}$$

$$K_{i-1} = B \cdot K_i + R \cdot I_{i-1} + E_i \tag{3.137}$$

The values B and R are the radiation transmission and the radiation reflection numbers of the respective layers. The transmission number B is a function of emissivity ε_r and porosity ε, and the reflection number R is calculated from B.

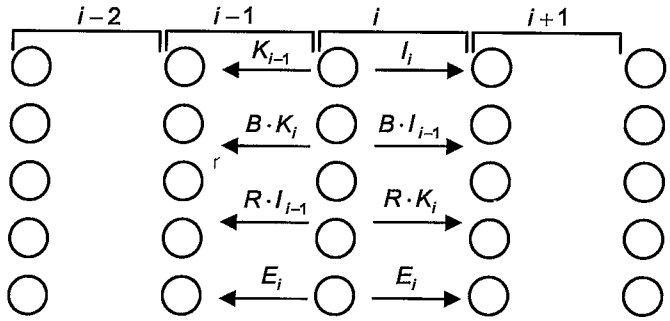

Figure 3.29: Layer model of Vortmeyer (for demonstrating radiation fluxes the layers are shown separated) (Vortmeyer, 1966:1).

Rearranging Eq. (3.136) and Eq. (3.137) for the emittance of pebble layer i yields the following:

$$E_i = I_i - B \cdot I_{i-1} - R \cdot K_i \tag{3.138}$$

$$E_i = K_{i-1} - B \cdot K_i - R \cdot I_{i-1} \tag{3.139}$$

The radiation transmission B and reflection R numbers are empirically calculated parameters, where B is plotted for a porosity range of between $\varepsilon = 0.40$ and 0.48 in Figure 3.30. The radiation reflection number R is a function of B as calculated by the following:

$$R = (1-B)(1-\varepsilon_r') \tag{3.140}$$

where

$$\varepsilon_r' = \frac{\varepsilon_r}{0.5(1-\varepsilon_r)+\varepsilon_r} \tag{3.141}$$

The emission of the layer E_i can now be obtained by the following:

$$E_i = (1-B-R)\sigma T_i^4 \tag{3.142}$$

where T_i is the temperature of the *i'th* layer. Vortmeyer (1966:1) assumed that the temperature is uniform within a layer and that the temperature changes through the packed bed from layer to layer.

Later Vortmeyer (1978:533) defined the radiation exchange factor to be:

$$F_E = \frac{2B + \varepsilon_r(1-B)}{2(1-B) - \varepsilon_r(1-B)} \tag{3.143}$$

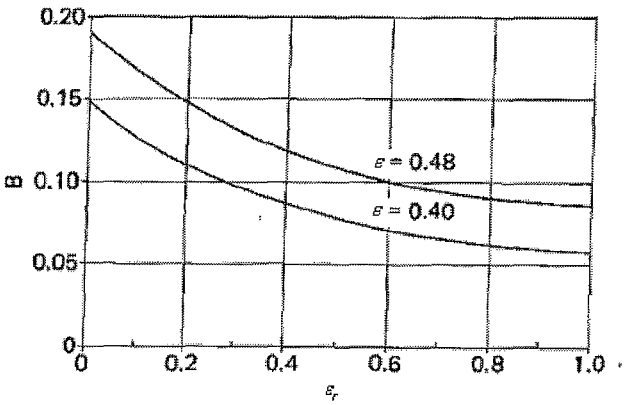

Figure 3.30: Radiation transmission number B (Vortmeyer & Boerner, 1966:1)

Breitbach (1978:1) introduced a new set of equations because he stated that at high temperatures and with low values of k_s the temperature gradient within a layer must be taken into account. The equation yields:

$$k_e^r = \left[\frac{\pi}{6}\frac{\psi}{1-\varepsilon}\cdot\left(1-\frac{\tau h(\Lambda_s,\varepsilon_r,\varepsilon)(1+\psi)}{1+\psi\tau h(\Lambda_s,\varepsilon_r,\varepsilon)}\right)\right]4\sigma T^3 d_p \tag{3.144}$$

where

$$\tau = \frac{1-B-R}{1+B-R} \tag{3.145}$$

$$\psi = \frac{1+B-R}{1-B+R} \tag{3.146}$$

$$h(\Lambda_s,\varepsilon_r,\varepsilon) = \left[1-2\frac{B(0)-B}{1-B-R}\right]\frac{\varepsilon_r'}{\frac{12}{\pi}\Lambda_s(1-\varepsilon)+\varepsilon_r'} \tag{3.147}$$

$$\Lambda_s = \frac{k_s}{4d_p\sigma T^3} \tag{3.148}$$

Extraction of the radiation exchange factor from Eq. (3.144) resulted in:

$$F_E^* = \left[\frac{\pi}{6}\frac{\psi}{1-\varepsilon}\cdot\left(1-\frac{\tau h(\Lambda_s,\varepsilon_r,\varepsilon)(1+\psi)}{1+\psi\tau h(\Lambda_s,\varepsilon_r,\varepsilon)}\right)\right] \tag{3.149}$$

The radiation transmission number $B(0)$ is for the case where $\varepsilon_r = 0$.

MODEL 4: Breitbach & Barthels (1980:392)

Breitbach & Barthels (1980:392) optimised the model presented by Zehner & Schlünder (1972:1303). They noted that an unsatisfactory feature of the Zehner & Schlünder (1972:1303) model is that the unit cell is assumed to be closed and therefore radiation from

the voids outside the unit cell is not taken into account. Breitbach & Barthels (1980:392) changed the correlation by changing the derivation, closing the base areas of the unit cell with black surfaces instead of surfaces with the same emittance as the spheres. This resulted in the following:

$$k_e^r = \left\{ \left[1-\sqrt{(1-\varepsilon)}\right]\varepsilon + \frac{\sqrt{(1-\varepsilon)}}{\frac{2}{\varepsilon_r}-1} \cdot \frac{B+1}{B} \cdot \frac{1}{1+\frac{1}{\left(\frac{2}{\varepsilon_r}-1\right)\Lambda_s}} \right\} 4\sigma T^3 d_p \tag{3.150}$$

$$\Lambda_s = \frac{k_s}{4\sigma T^3 d_p} \tag{3.151}$$

$$B = 1.25\left(\frac{1-\varepsilon}{\varepsilon}\right)^{10/9} \tag{3.152}$$

Experimental results were obtained by using a transient method to determine the effective thermal conductivity in packed beds of graphite and zirconium oxide spheres under vacuum conditions at temperatures up to 1000°C and 1500°C, respectively. In their assumptions, they disregarded any contribution that point contact conduction may have on the experimental results. They found that the theoretical values of k_e^r predicted by the Zehner & Schlünder (1972:1303) model are too low, while the values predicted by the model of Vortmeyer (1966:1) are somewhat too high. Breitbach & Barthels (1980:392) further demonstrated that the modified correlation presented in Eq. (3.150) yielded a better fit to the experimental data. Extracting the radiation exchange factor from Eq. (3.150) yields the following:

$$F_E^* = \left\{ \left[1-\sqrt{(1-\varepsilon)}\right]\varepsilon + \frac{\sqrt{(1-\varepsilon)}}{\frac{2}{\varepsilon_r}-1} \cdot \frac{B+1}{B} \cdot \frac{1}{1+\frac{1}{\left(\frac{2}{\varepsilon_r}-1\right)\Lambda_s}} \right\} \tag{3.153}$$

MODEL 5: Robold (1982:1)

Since Vortmeyer (1966:1) presented his model, various researchers such as Breitbach, (1978:1) and Kasparek (1975:1) optimised specific aspects of the model. One feature that became clear is that after each optimisation process the graph describing the empirical radiation transmission number B changed. Robold (1982:129) also optimised Vortmeyer's (1966:1) model by introducing a transformed pebble diameter d^{ε}, a fluid gap width d_f^{ε} and a solid thickness parameter d_s^{ε}. It must, however, be noted that this model presented below

and all its predecessors is only valid for the bulk region of a randomly packed bed. The porous layers are displayed graphically in Figure 3.31.

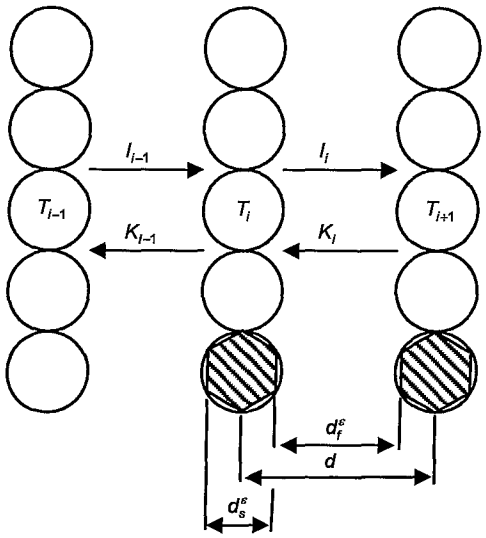

Figure 3.31: Added parameters by Robold to Vortmeyer's model (Robold, 1982:148; Vortmeyer, 1966:1)

Robold (1982:129), like Breitbach & Barthels (1980:392), took the temperature gradient in each layer into account and claimed that the model is only valid when the temperature gradient over each layer is smaller than the average temperature, so that $\Delta T/\overline{T} < 1$. The transformed pebble diameter is defined as:

$$d^\varepsilon = \frac{(1-\varepsilon_{SC})}{(1-\varepsilon)} d_p = \frac{(1-0.477)}{(1-\varepsilon)} d_p = \frac{0.523}{(1-\varepsilon)} d_p \tag{3.154}$$

Although the porosity for a SC packing is $\varepsilon_{SC} = \left(1-\frac{\pi}{6}\right) = 0.476$, Robold (1982:23) assumed it to be 0.477.[6] Therefore, for consistency in presenting his model, $\varepsilon_{SC} = 0.477$ is assumed. Again, an analogy between ordered packings and a randomly packed bed is made. In more general terms d^ε is given by:

$$d^\varepsilon = d_f^\varepsilon + d_s^\varepsilon \tag{3.155}$$

The fluid gap width d_f^ε and solid thickness parameter d_s^ε can be calculated by the following:

$$d_f^\varepsilon = \frac{d^\varepsilon}{1+\pi} \tag{3.156}$$

$$d_s^\varepsilon = d^\varepsilon \frac{\pi}{1+\pi} \tag{3.157}$$

[6] Robold (1982:23) did not round off the packing density to three digits after the decimal point.

The radiation exchange factor is given by:

$$F_E = \frac{2B + \varepsilon_r(1-B)}{(1-B)(2-\varepsilon_r)} \tag{3.158}$$

also

$$F_{E,0} = F_E(B=0) = \frac{\varepsilon_r}{2-\varepsilon_r} \tag{3.159}$$

Robold (1982:39) introduced a radiation exchange ratio, which can be obtained by:

$$\chi = \frac{F_{E,0}}{F_E} \tag{3.160}$$

As previously mentioned, the empirical transmission number B in Eq. (3.158) differs from that displayed in Figure 3.30. The transmission number required for the Robold model can be obtained from Figure 3.32 (a) and (b).

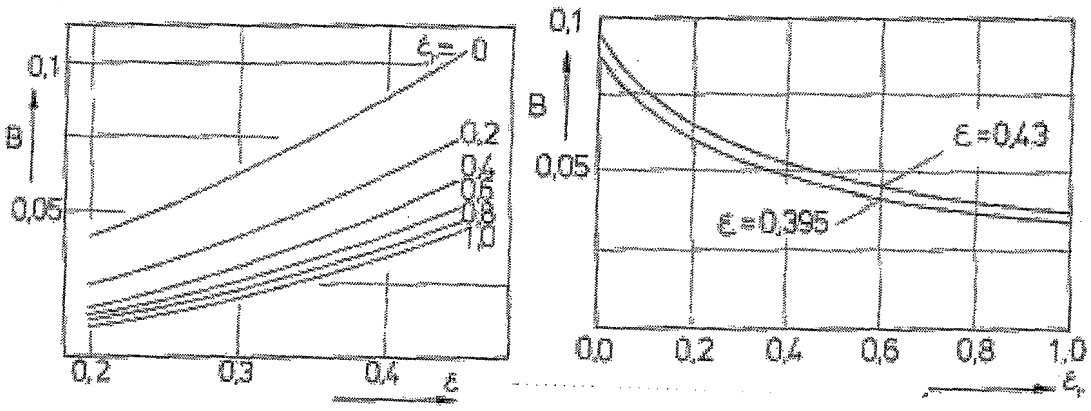

(a) (b)

Figure 3.32: Transmission number versus (a) porosity and (b) emissivity (Robold, 1982:151)

Furthermore, Robold (1982:129) introduced a dimensionless weighting function:

$$\Delta_0 = \frac{F_E\left[1-B(0,\varepsilon)\right]-B(0,\varepsilon)}{F_{E,0}\left[1-B(0,\varepsilon)\right]} \tag{3.161}$$

The effective thermal conductivity is then given by:

$$k_e^{g,r} = F_E\left[1-\chi\frac{\Delta_0}{1+\dfrac{k_s/d_s^\varepsilon}{F_{E,0}4\sigma T^3+k_f/d_f^\varepsilon}}\right]4d^\varepsilon\sigma T^3 + k_f\frac{d^\varepsilon}{d_f^\varepsilon}\left[1-\frac{\Delta_0}{1+\dfrac{k_s/d_s^\varepsilon}{F_{E,0}4\sigma T^3+k_f/d_f^\varepsilon}}\right] \tag{3.162}$$

Robold (1982:102) also introduced a contact area parameter by assuming an empirical value

$s = 0.0035$. This value is incorporated into the following formula:

$$k_{eff} = (1-s)k_e^{g,r} + sk_s \tag{3.163}$$

where $k_e^{g,r}$ is calculated by Eq. (3.162). Extracting the radiation exchange factor F_E^* from Eq. (3.162) yields the following:

$$F_E^* = F_E\left[1-\chi\frac{\Delta_0}{1+\dfrac{k_s/d_s^\varepsilon}{F_{E,0}4\sigma T^3+k_f/d_f^\varepsilon}}\right] \tag{3.164}$$

The fluid/gas conductivity k_f is present in Eq. (3.164). However, this cannot be the case in a vacuum bed; therefore, Eq. (3.164) reduces to:

$$F_E^* = F_E\left[1-\chi\frac{\Delta_0}{1+\dfrac{k_s}{F_{E,0}4d_s^\varepsilon\sigma T^3}}\right] \tag{3.165}$$

MODEL 6: Singh & Kaviany (1994:2579)

Singh & Kaviany (1994:2579) assumed that a packed bed can be divided into layers of spheres. The purpose of their study was to calculate the radiant exchange factor F_E^* using a ray tracing technique with a Monte Carlo approach. Results were obtained and empirical curve fits were generated for a SC packed bed of $\varepsilon = 0.476$ from dimensionless charts such as that presented in Figure 3.33. The following empirical correlation for the radiant exchange factor was derived with the constants given in Table 3.5:

$$F_E^* = a_1\varepsilon_r \tan^{-1}\left(a_2\frac{(\Lambda_s)^{a_3}}{\varepsilon_r}\right) + a_4 \tag{3.166}$$

Table 3.5: Constants for the radiation exchange factor Eq. (3.166) (Singh & Kaviany, 1994:2583)

VARIABLE	SPECULAR SURFACE	DIFFUSE SURFACE
a_1	0.5711	0.5756
a_2	1.4704	1.5353
a_3	0.8237	0.8011
a_4	0.2079	0.1843

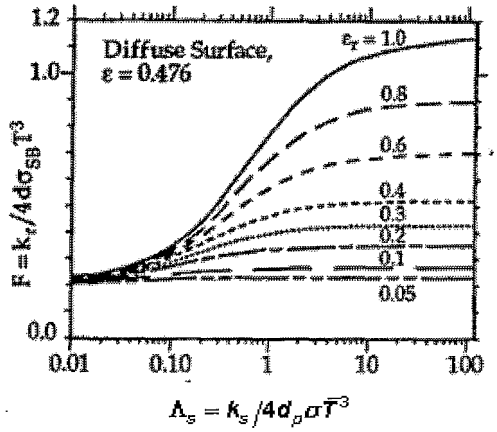

Figure 3.33: Radiation exchange factor versus dimensionless solid conductivity (Singh & Kaviany, 1994:2582)

MODEL 7: Cheng et al. (2002:1)

Although this model is based on a numerical approach, several points are worth noting. This model is an extension of Model 9 in Section 3.2.1. Cheng *et al.* (2002:1) approached the simulation of a randomly packed bed of mono-sized spheres by basing their model on the Voronoi tessellation theory. They state that heat is transported within a Voronoi polyhedron and between neighbouring Voronoi polyhedra, which means ultimately an increased focus on packing structure. The radiation heat transfer between spheres i and j can be quantified based on the double taper cone model shown in Figure 3.34, under the following assumptions:

1. Sphere diameter is much larger than wavelength of radiation.
2. Sphere surface is gray emitting.
3. Sphere is an opaque solid.
4. $\Delta T/T$ is much less than 1 across a sphere layer.
5. The imaginary surface R (ACBB'C'A') is perfectly insulated and diffusely reflective.

For mono-sized spheres of the same properties the following was obtained:

$$Q_{ij,rad} = \frac{\sigma\left(T_i^4 - T_j^4\right)}{2\dfrac{1-\varepsilon_{r,i}}{\varepsilon_{r,i}A_i} + \dfrac{A_i\left(1-F_{ij}\right)}{2}} \qquad (3.167)$$

Radiation exchange area A_i depends on the geometric configuration around spheres i and j, which can be derived directly from the packing structure. F_{ij}, the view factor between surface AA' and BB', can be obtained by extending the numerical integral method of Jones (1965:421). When they compared their results with Yagi & Kunii's (1957:373) vacuum experimental data, Cheng *et al.* (2002:1) obtained relatively good agreement.

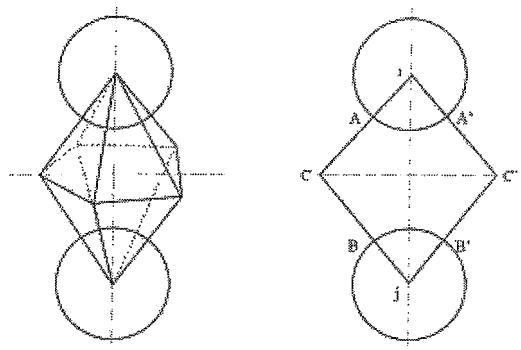

(a) Double pyramid model (b) Double taper cone model

Figure 3.34: Connecting models between two neighbouring Voronoi polyhedra (Cheng *et al.*, 2002:1)

3.2.4 EFFECTIVE THERMAL CONDUCTIVITY AT THE NEAR-WALL INTERFACE

It is evident from the previous sections that a large number of correlations have been developed to calculate the effective thermal conductivity in a stagnant fluid or gas environment. Although not explicitly noted, it appears from open literature that these correlations have also been used to compute the effective thermal conductivities for stagnant flow with large porosity variations particularly in the near-wall region.

Thurgood *et al.* (2004:1) assessed the applicability of the effective thermal conductivity correlations in the near-wall region by considering the correlations developed by Kunii & Smith (1960:71), Zehner & Schlünder (1970:933), and Bauer & Schlünder (1978:189). This work resulted in a clear demonstration of the lack of validity of these correlations in the near-wall region.

Thurgood *et al.* (2004:1), Vortmeyer (1978:533) and Robold (1982:155) argued that the temperature is only affected in the wall region $1/2d_p$ away from the wall. Their argument is that the reactor wall forces the spheres in contact with the wall into a nearly ordered arrangement (pebble centre $1/2d_p$ away from the wall). Thus, each pebble touches the wall through one contact point. This solitary contact with the wall greatly reduces heat flow from the pebble to the wall.

This argument was based on experimental work from Kasparek & Vortmeyer (1976:117) and the SANA-I experimental data, which observed a temperature jump $1/2d_p$ from the wall. However, it must be emphasised that a problem with these experimental test facilities is that they did not have enough temperature measurements in the radial direction to observe a

decline in the effective thermal conductivity further away from the wall (near-wall region). In this section, three models that attempt to quantify the wall region are discussed. No models were found in open literature addressing the calculation of the effective thermal conductivity in the near-wall region of a randomly packed bed.

MODEL 1: Yagi & Kunii (1961:760)

Yagi & Kunii (1961:760) modified the correlation presented by Kunii & Smith (1960:71) for the near-wall region by the development of the following:

$$\frac{k_{e,NW}^{g}}{k_f} = \varepsilon_{wall}\left[2+\frac{k_{rs}d_p}{k_f}\right]+\frac{\beta\left(1+\varepsilon_{wall}\right)}{\left[\dfrac{1}{1/\psi_{wall}+k_{rs}d_p/k_f}+\dfrac{\gamma}{\kappa}\right]} \tag{3.168}$$

where $\gamma = 1/3$ and

$$\psi_{wall} = \frac{1}{4}\frac{\left(\dfrac{(\kappa-1)}{\kappa}\right)^2}{\ln\kappa-\dfrac{(\kappa-1)}{\kappa}}-\frac{1}{3\kappa} \tag{3.169}$$

The definition of k_{rv} and k_{rs} can be calculated using Eq. (3.131) and Eq. (3.132). It is important to note that Yagi & Kunii (1961:760) assumed a constant mean near-wall porosity of $\varepsilon_{wall} = 0.7$.

MODEL 2: Robold (1982:1)

As previously mentioned, Robold (1982:155) assumed the wall region to be a distance of $1/2d_p$ away from the wall. He introduced a correlation to calculate the effective thermal conductivity for the wall region using the same method described in Section 3.2.3.

The transformed pebble diameter d_W^{ε} for the wall region is given by:

$$d_W^{\varepsilon} = d_{W,f}^{\varepsilon} + d_{W,s}^{\varepsilon} \tag{3.170}$$

as well as:

$$d_W^{\varepsilon} = \frac{\varepsilon_W}{\varepsilon}\frac{d^{\varepsilon}}{2} \tag{3.171}$$

The fluid gap width $d_{W,f}^{\varepsilon}$ and the solid thickness parameter in the wall region $d_{W,s}^{\varepsilon}$ can be calculated by the following:

$$d_{W,f}^{\varepsilon} = \frac{\varepsilon_W}{\varepsilon}\frac{d_f^{\varepsilon}}{2} \tag{3.172}$$

$$d_{W,s}^{\varepsilon} = \frac{\varepsilon_W}{\varepsilon}\frac{d_s^{\varepsilon}}{2} \tag{3.173}$$

where ε_W is obtained from an empirical graph generated from a comparison with experimental data. The radiation exchange factor can be calculated by the following:

$$F_W = \frac{\left(1-R-R^W+RR^W\right)\left(1+B-RR^W\right)}{\left(1-B+RR^W\right)\left(1-B+RR^W\right)-4RR^W} \tag{3.174}$$

where

$$R = (1-B)(1-\varepsilon_r) \tag{3.175}$$

and

$$R^W = \left(1-\varepsilon_r^W\right) \tag{3.176}$$

also

$$F_{W,0} = \frac{1}{\frac{1}{\varepsilon_r}+\frac{L}{\varepsilon_r^W}-1} \tag{3.177}$$

Robold (1982:2751) also introduced a radiation exchange factor ratio, which can be obtained by:

$$\chi_W = \frac{\left(\eta_1^W+\vartheta_1^W\right)+\left(\eta_2^W+\vartheta_2^W\right)}{2}\frac{d_W^{\varepsilon}}{2} \tag{3.178}$$

where

$$\eta_1^W = \frac{(1-B)\varepsilon_r}{(1+B)-R^WR}\frac{2}{d_W^{\varepsilon}} \qquad \vartheta_1^W = \frac{R\varepsilon_r^W}{(1-B)-R^WR}\frac{2}{d_W^{\varepsilon}} \tag{3.179}$$

$$\eta_2^W = \frac{(1+B)\varepsilon_r^W}{(1+B)-R^WR}\frac{2}{d_W^{\varepsilon}} \qquad \vartheta_2^W = \frac{R^W(1-B)\varepsilon_r}{(1+B)-R^WR}\frac{2}{d_W^{\varepsilon}} \tag{3.180}$$

Furthermore, Robold. (1982:2751) introduced a dimensionless weighting function:

$$\Delta_0 = \frac{2F_W\left(\varepsilon_r^W/\varepsilon_r=1\right)\left[1-B(\varepsilon_r,\varepsilon)\right]-B(0,\varepsilon)}{2F_{W,0}\left[1-B(0,\varepsilon)\right]} \tag{3.181}$$

The effective thermal conductivity for $1/2d_p$ away from the wall is then given by:

$$k_{W,e} = 4F_W \left[1 - \chi_W \frac{\Delta_{W,0}}{1 + \dfrac{k_s / d^{\varepsilon}_{W,s}}{4F_{W,0}\sigma T_W^3 + k_f / d^{\varepsilon}_{W,f}}} \right] d^{\varepsilon}_W \sigma T_W^3 + k_f \frac{d^{\varepsilon}}{d^{\varepsilon}_f} \left[1 - \frac{\Delta_{W,0}}{1 + \dfrac{k_s / d^{\varepsilon}_{W,s}}{4F_{W,0}\sigma T_W^3 + k_f / d^{\varepsilon}_{W,f}}} \right] \tag{3.182}$$

MODEL 3: Tsotsas (2002:2.8.2)

Tsotsas (2002:2.8.2) proposed a modification to the Bauer & Schlünder (1978:189) correlation to be used in the near-wall region. The first step in the procedure is to compute the effective thermal conductivity according to Eq. (3.90) with $\kappa_r = 0$. This quantity is then termed $k^{g,c}_{e,0}$. Then the near-wall effective thermal conductivity is calculated by the following:

$$k_{eff,NW} = k^{g,c}_{e,0} + \left(1 - \sqrt{1-\varepsilon}\right)\kappa_r + \sqrt{1-\varepsilon}\left(\frac{1}{\kappa_r} + \frac{1}{k_p}\right)^{-1} \tag{3.183}$$

Thurgood *et al.* (2004:1) stated that that the modified correlation is not continuous with the parent Bauer & Schlünder (1978:189) correlation.

3.3 STATISTICAL APPROACH

Lu (2000:12) stated that statistical models are very different from the deterministic models and are a relatively new means of investigating heat transfer in packed beds. Deterministic models have been used for far longer. Torquato (1987:151) provided a good survey of the available statistical models for determining the effective thermal and electrical conductivity, dielectric constants and magnetic permeability of a porous matrix.

Results from his model show good agreement with experimental data, on condition that $\kappa = k_s / k_f$ is low. As κ increases, Torquato's (1987:151) model tends to under-predict the effective conduction values versus experimental studies. He attributes this to the microstructural differences between the model and the experiment and the inaccuracy of superposition approximation, which he used to calculate the three-point parameter characterising the microstructure of porous media.

Nayak & Tien (1978:669) also considered the heat flow in packed beds consisting of spheres

with a statistical approach. Their theory establishes the local coordination number as the suitable statistical variable and predicts the coordination number frequency in the bulk region for a randomly packed bed. Heat conduction through spheres in contact is then represented analytically by a network of thermal resistances in series and parallel. The theory was originally developed for the case of a randomly packed bed with non-uniform pebble diameters. However, results were also generated for pebbles with uniform diameters.

3.4 COMPARISON BETWEEN EFFECTIVE THERMAL CONDUCTIVITY MODELS

Despite decades of experimental and theoretical work, predicting the effective thermal conductivity of porous media saturated with a fluid continues to be a significant problem in heat transfer, according to Aichlmayr & Kulacki (2006:377). The problem is unsolved because the effective thermal conductivity is a phenomenological characterisation of a solid-fluid medium rather than a thermo-physical property. Aichlmayr & Kulacki (2006:377) argued that physical limits are established representing the effective thermal conductivity data in saturated porous media by the parallel and series method. They also stated that our understanding of the effective thermal conductivity in large solid-fluid conductivity ratio $\kappa > 10^3$ media is incomplete.

The generally accepted method to compare the effective thermal conductivity data (disregarding thermal radiation) is to normalise the solid effective thermal conductivities with the fluid thermal conductivities, subsequently generating a dimensionless chart. In this section a number of these charts generated by the author as a part of this study are presented in order to compare and evaluate the different models discussed earlier.

Experimental measurements for any porous media arrangement saturated with a stagnant fluid should fall inside the minimum and maximum bounds proposed by Deissler & Boegli (1958:1417), on condition that no natural convection occurs. The bounds are displayed in Figure 3.35 together with various other models. Aiclmayr (1999:36) noted that even though the literature abounds with measurements of the effective thermal conductivity, it lacks uncertainty estimates for experimental results. Hence, the quality of the measurements presented in the literature is undetermined. Nonetheless, experimental measurements are also displayed in Figure 3.35 for different porosities and sphere diameter arrangements obtained from Aichlmayr & Kulacki (2006:377), Prasad *et al.* (1989:1793) and Nozad *et al.* (1985b:857).

Nield (1991:1575), however, questioned the accuracy of the experimental results published by Prasad *et al.* (1989:1793) for $\kappa < 1$ because he noted that several of the effective thermal

conductivity ratios are not within the bounds of maximum and minimum values given by the series and parallel models as shown in Figure 3.35. However, for the purpose of this study, we leave the data as published. An in-depth analysis into the experimental measurements for saturated porous media is given in Aichlmayr & Kulacki (2006:377).

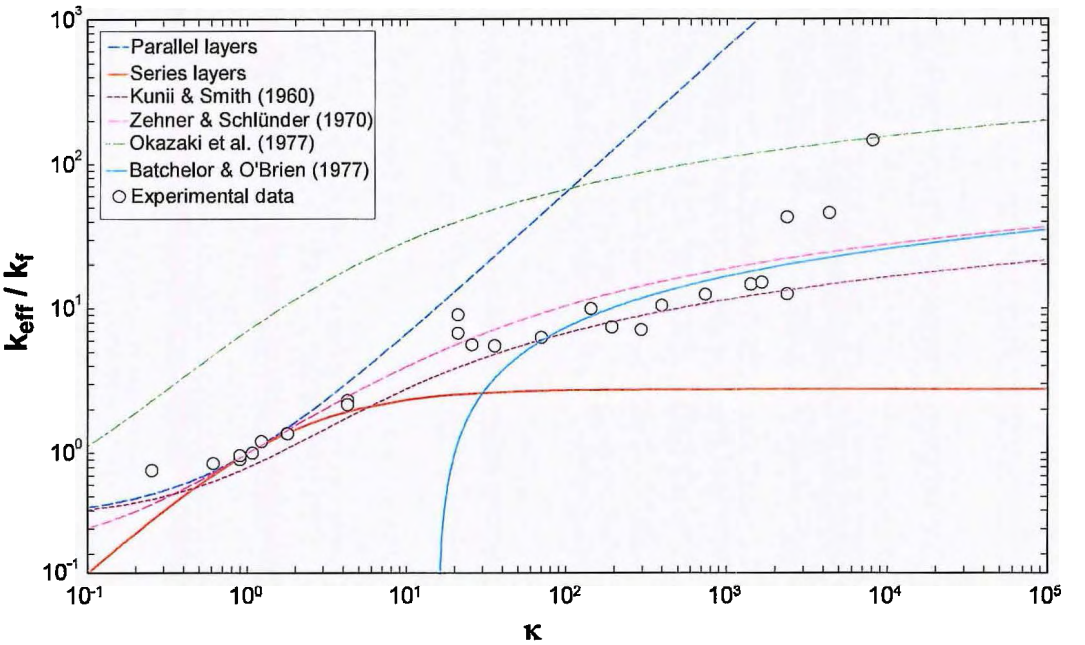

Figure 3.35: Effective thermal conductivity, k_e^g, models at $\varepsilon = 0.36$ versus experimental data

Figure 3.35 demonstrates the failure of the Kunii & Smith (1960:71), Zehner & Schlünder (1970:933), Okazaki *et al.* (1977:164) and Batchelor & O'Brien (1977:313) models when $\kappa > 10^3$. The inability of these models to simulate the effective thermal conductivity data can be linked to the disregard of the details of the contact area. Therefore, incorporating the contact area parameters led to results displayed in Figure 3.36.

The models proposed by Hsu *et al.* (1995:264) and Zehner & Schlünder (1970:933) + Kavainy (1991:127) and co-workers correspond well to the experimental data presented in Figure 3.36. On the contrary, it should be noted that each of these models has a unique contact area variable to obtain agreement with the experimental data. Each parameter was evaluated and adjusted to obtain the best fit with the experimental data. A summary of these parameters is displayed in Table 3.6.

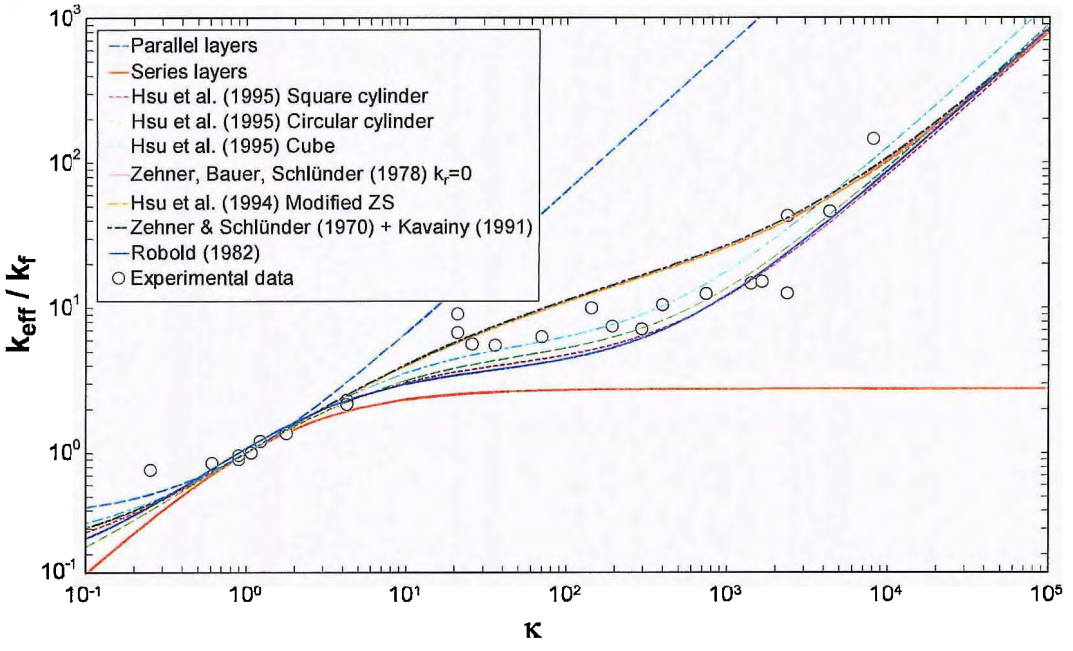

Figure 3.36: Effective thermal conductivity $k_e^{g,c}$ models at $\varepsilon = 0.36$ versus experimental data[7]

Table 3.6: Contact area constants for models evaluated in Figure 3.36

RESEARCHER	CONTACT AREA PARAMETER
Hsu *et al.* (1995:264) Square cylinder	$\gamma_c = 0.01$
Hsu *et al.* (1995:264) Circular cylinder	$\gamma_c = 0.01$
Hsu *et al.* (1995:264) Cube	$\gamma_c = 0.13$
Bauer & Schlünder (1978:189)	$\varphi = 0.01$
Hsu *et al.* (1994:2751)	$\alpha_0 = 0.002$
Zehner & Schlünder (1970:933) + Kaviany (1991:127)	$p = 2 \times 10^3$ [*Pa*]
Robold (1982:102)	$s = 0.0085$

It is important to note that the second part of Robold's (1982:128) correlation, Eq. (3.162), was used for the analysis in Figure 3.36, as well as an average emissivity of $\bar{\varepsilon}_r = 0.88$.

Another important aspect to be addressed is that of the applicability envelope of the effective thermal conductivity models with variation in porosity. The porosity in Figure 3.37 was varied between $0.2595 \le \varepsilon \le 1$ for one fixed value of $\kappa = 488.5$.

[7] Aichlmayr and Kulacki (2006:439) state that the circular cylinder model gives unrealistic estimates for $\kappa < 100$. However, that is not the case. Presumably, an error was made in their programming of the formula.

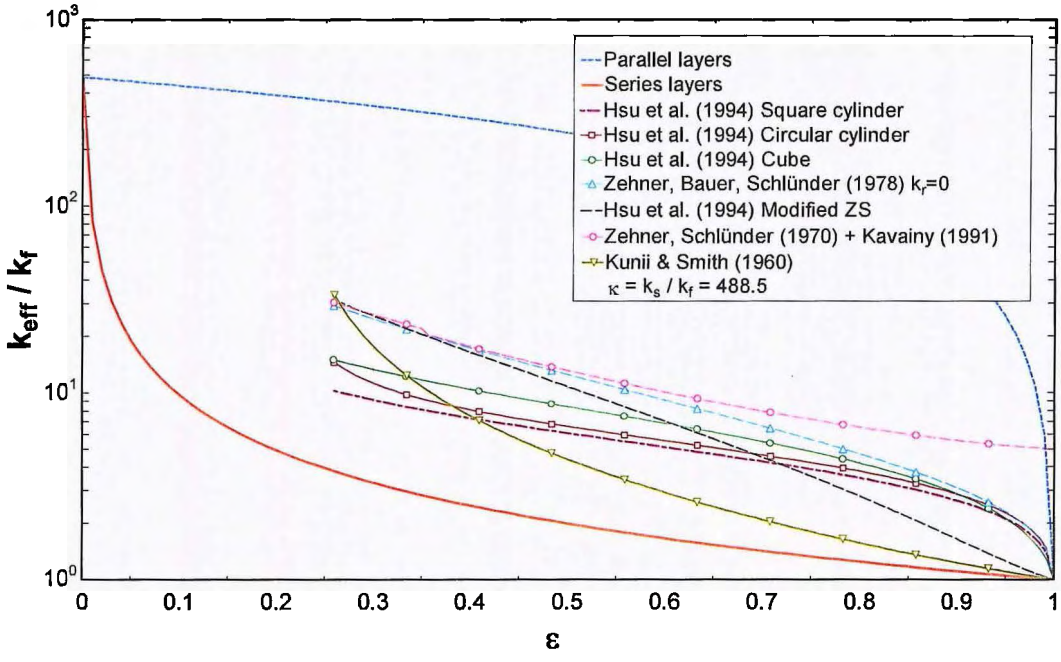

Figure 3.37: Effective thermal conductivity models (contact area included, no radiation) versus porosity variation, $(\kappa = 488.5)$

In Figure 3.37 the assignment of certain parameters to a specified porosity range in the Kaviany (1991:127) model is the reason that the summation of the Zehner & Schlünder (1970) and Kaviany (1991) models does not approach the fluid conductivity when $\varepsilon = 1$ as would be expected.

The next aspect to consider comparing is thermal radiation. Researchers such as Vortmeyer (1978:532) recognised the importance of the contribution of thermal radiation to the overall effective thermal conductivity k_{eff} at high temperatures. However, there is little experimental data available for such research.

Cheng *et al.* (2002:1) noted that since the original proposal by Chen & Churchill (1963:35) many models have been proposed that calculate the homogeneous radiation exchange factor F_E and F_E^*. However, Cheng *et al.* (2002:1) further stated that the structure of a packed bed and its effect on radiation heat transfer cannot be fully represented by F_E or F_E^*. In fact, a unit cell model has never taken into account the long-range radiation effects through the void spaces in between spheres, which must exist in packed beds (Vortmeyer, 1978:532). Nonetheless, Table A.1 gives a summary of the investigated radiation exchange factors, as well as results obtained by different numerical and experimental methods.

One experimental exercise worth mentioning is that of Kasparek & Vortmeyer (1976:117) who

studied the radiation heat transfer in a packed bed where contact area was eliminated. Radiation heat transfer measurements were taken through a number of sphere layers connected to strings where conduction and convection were also eliminated by introducing a small gap between sphere layers in vacuum conditions, which ultimately resulted in obtaining radiation exchange factor measurements F_E for different emissivities and porosities. Comparing F_E and F_E^* models displayed in Table A.1 with experimental data from Kasparek & Vortmeyer (1976:117) yields Figure 3.38.

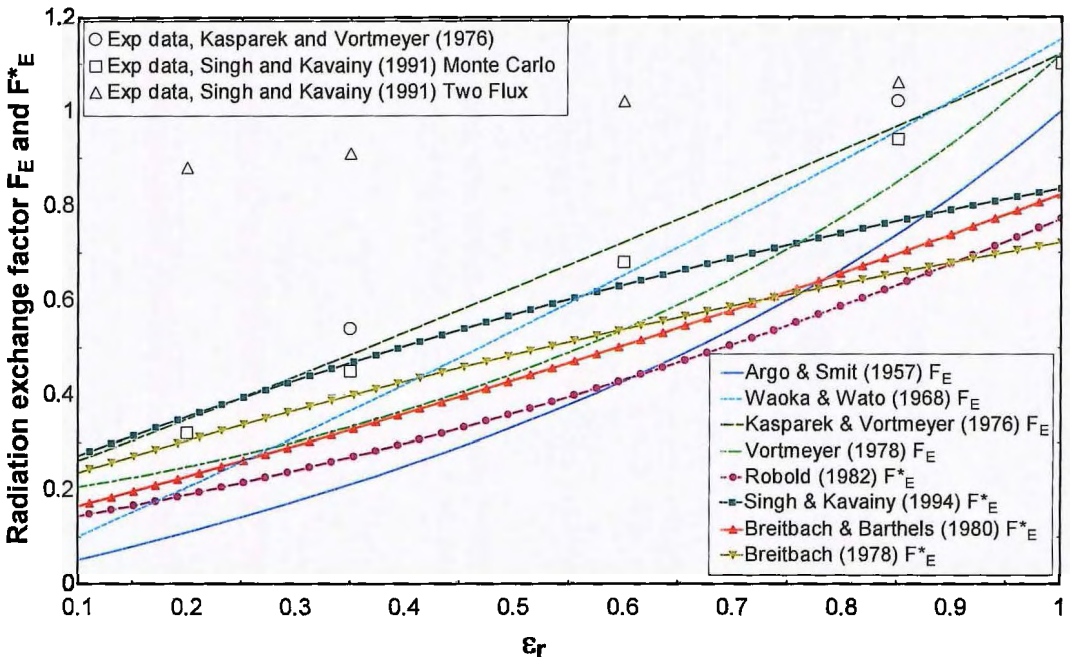

Figure 3.38: Comparison of F_E and F_E^* models with emissivity with $T = 1067\,°C$, $\varepsilon = 0.43$ and $k_s = 30[W/mK]$

Figure 3.38 clearly demonstrates a difference between the F_E and F_E^* models and the experimental data generated by Kasparek & Vortmeyer (1976:117). Also, comparison of the results between the Two-flux Model and the Monte Carlo Diffuse Model shows that the Two-flux Model yields unrealistic values at low emissivities ε_r.

3.5 CONCLUSION

This chapter presented an in-depth analysis of the models found in open literature to calculate the effective thermal conductivity for mono-sized spheres. This research was intentionally done in such detail to highlight various uncertainties and limitations of the existing models, such as the difference between porosity and packing structure, as well as a lack of detailed simulation models for $50°C \leq T \leq 1600°C$.

It has been shown that relatively good accuracy can be obtained with several unit cell approaches in the bulk region of a packed bed, but that significant uncertainty arises in the near-wall and wall regions. The reason for the large uncertainty is the generalisation of various transport phenomena using empirical correlations for both heat transfer and packing structure.

Therefore, for annular PBRs a need exists for a new method to simulate the effective thermal conductivity that must address the porous structure in a more fundamental manner, especially in the near-wall regions. It has also been found that existing experimental data is insufficient to extract the effective thermal conductivity in the near-wall region. This highlights the need for an experiment with detailed temperature measurements to have a better indication of the effective thermal conductivity in the bulk, near-wall and wall regions. A summary of the literature survey done in Chapter 3 and relevant literature is illustrated in Figure 3.39.

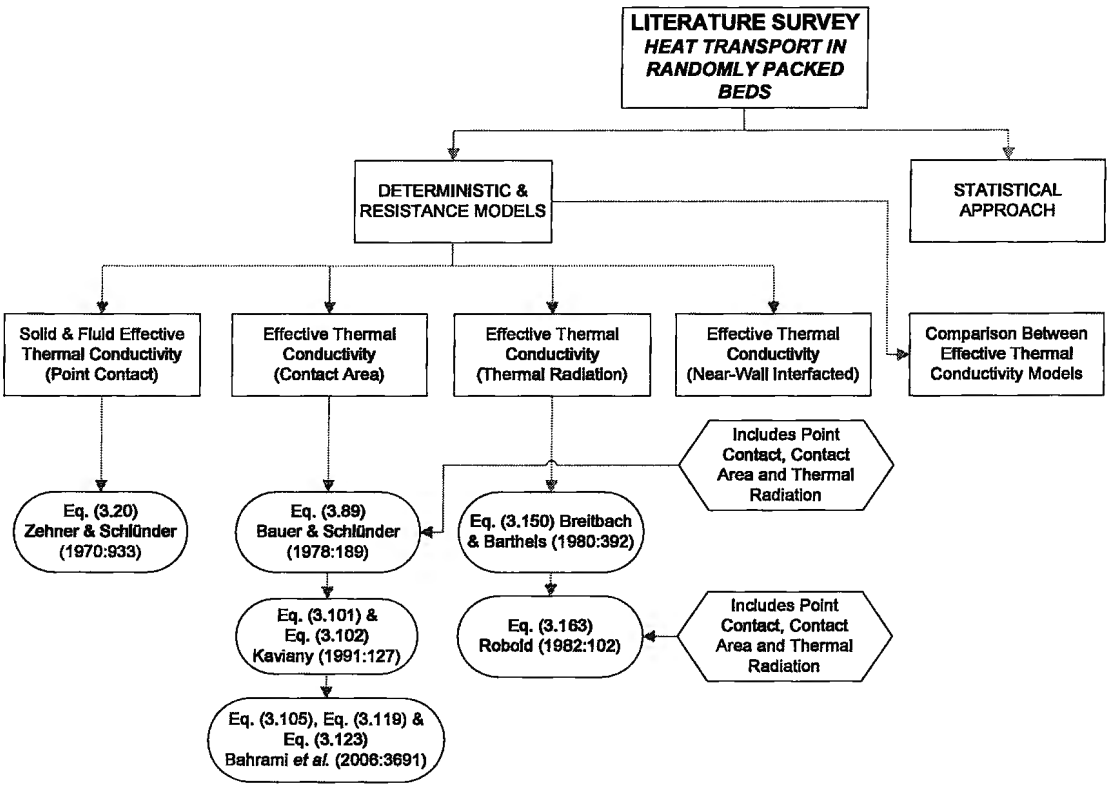

Figure 3.39: Literature survey heat transport in randomly packed beds flowchart